Environment International 129 (2019) 408–422

Contents lists available at ScienceDirect

Environment International

journal homepage: www.elsevier.com/locate/envint

Bayesian evaluation of a physiologically based pharmacokinetic (PBPK) model for perfluorooctane sulfonate (PFOS) to characterize the interspecies uncertainty between mice, rats, monkeys, and humans: Development and performance verification

Wei-Chun Chou, Zhoumeng Lin*

Institute of Computational Comparative Medicine (ICCM), Department of Anatomy and Physiology, College of Veterinary Medicine, Kansas State University, Manhattan, KS 66506, United States

ARTICLE INFO

Handling editor: Martí Nadal

Keywords:
Interspecies extrapolation
Markov chain Monte Carlo (MCMC)
Perfluoroalkyl substances (PFAS)
Perfluorooctane sulfonate (PFOS)
Physiologically based pharmacokinetic (PBPK) modeling
Risk assessment

ABSTRACT

A challenge in the risk assessment of perfluorooctane sulfonate (PFOS) is the large interspecies differences in its toxicokinetics that results in substantial uncertainty in the dosimetry and toxicity extrapolation from animals to humans. To address this challenge, the objective of this study was to develop an open-source physiologically based pharmacokinetic (PBPK) model accounting for species-specific toxicokinetic parameters of PFOS. Considering available knowledge about the toxicokinetic properties of PFOS, a PBPK model for PFOS in mice, rats, monkeys, and humans after intravenous and oral administrations was created. Available species-specific toxicokinetic data were used for model calibration and optimization, and independent datasets were used for model evaluation. Bayesian statistical analysis using Markov chain Monte Carlo (MCMC) simulation was performed to optimize the model and to characterize the uncertainty and interspecies variability of chemical-specific parameters. The model predictions well correlated with the majority of datasets for all four species, and the model was validated with independent data in rats, monkeys, and humans. The model was applied to predict human equivalent doses (HEDs) based on reported points of departure in selected critical toxicity studies in rats and monkeys following U.S. EPA's guidelines. The lower bounds of the model-derived HEDs were overall lower than the HEDs estimated by U.S. EPA (e.g., 0.2 vs. 1.3 μg/kg/day based on the rat plasma data). This integrated and comparative analysis provides an important step towards improving interspecies extrapolation and quantitative risk assessment of PFOS, and this open-source model provides a foundation for developing models for other perfluoroalkyl substances.

1. Introduction

Perfluorooctane sulfonate (PFOS) is a persistent organic pollutant that is used in a wide variety of consumer products, including cookware, furniture, household cleaners, and clothing; and it has been found to be ubiquitous in the environment (ATSDR, 2018). Due to its long half-life in humans (Olsen et al., 2007), environmental persistence, confirmed human environmental and occupational exposures (Calafat et al., 2006; Calafat et al., 2007; Olsen et al., 2003b; Olsen et al., 2008), as well as reported mammalian toxicity (Elcombe et al., 2012a; Seacat et al., 2003; Seacat et al., 2002), the potential risk of PFOS has become a public health concern. However, because of its substantial interspecies differences in toxicokinetics, its risk assessment and dosimetry extrapolation between animals and humans are difficult and of high uncertainty, which can be addressed through a physiologically based pharmacokinetic (PBPK) model that is validated in multiple species.

PFOS is known to be well absorbed in the gastrointestinal tract following oral exposure (Chang et al., 2012), minimally metabolized,

Abbreviations: ASC, average serum concentration; AUC, area under the curve; HED, human equivalent dose; EFSA, European Food Safety Authority; IV, intravenous; MCMC, Markov chain Monte Carlo; MOA, Mode of action; NOAEL, no-observed-adverse-effect-level; OATs, organic anion transporters; PBPK, physiologically based pharmacokinetic; PFOA, perfluorooctanoic acid; PFOS, perfluorooctane sulfonate; POD, point of departure; PTCs, proximal tubule cells; RfD, reference dose; TK, toxicokinetic; U.S. EPA, United States Environmental Protection Agency; WHO, World Health Organization

* Corresponding author at: 1800 Denison Avenue, P200 Mosier Hall, Institute of Computational Comparative Medicine (ICCM), Department of Anatomy and Physiology, College of Veterinary Medicine, Kansas State University, Manhattan, KS 66506, United States.

E-mail addresses: weichunc@vet.k-state.edu (W.-C. Chou), zhoumeng@ksu.edu (Z. Lin).

https://doi.org/10.1016/j.envint.2019.03.058
Received 19 January 2019; Received in revised form 7 March 2019; Accepted 25 March 2019

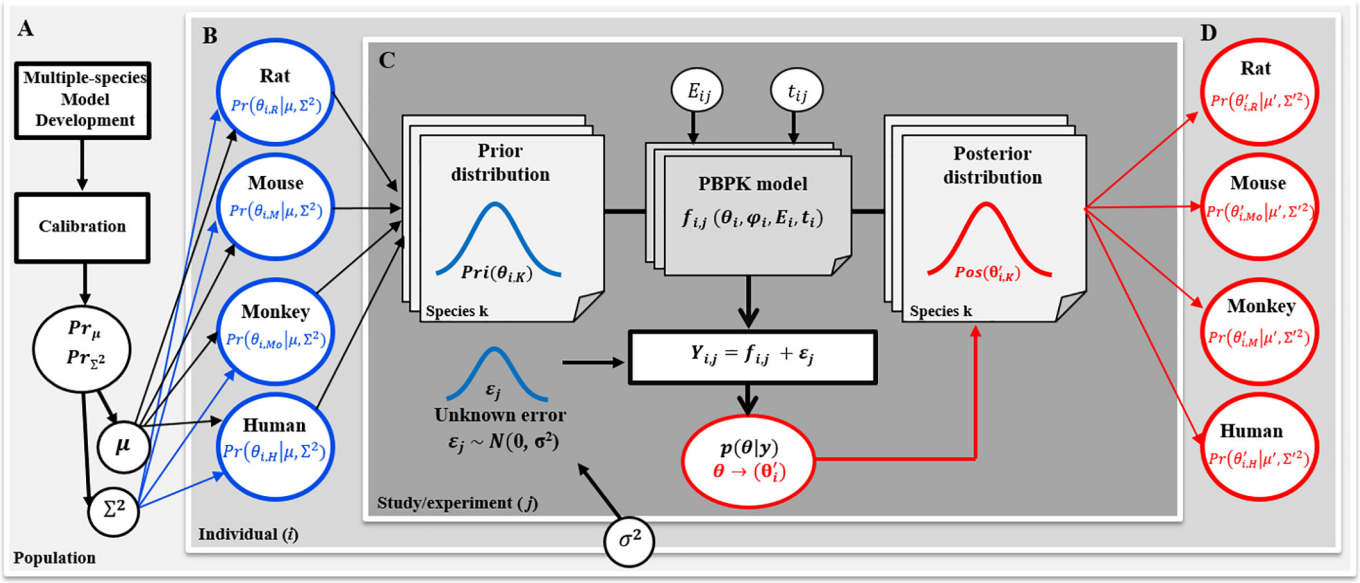

Fig. 1. Schematic illustration of the Bayesian-MCMC PBPK modeling approach. (A) The first step for model development and calibration is to obtain estimated parameters as prior information for subsequent MCMC analysis. (B) The second step is to define a prior distribution for each of the variable parameters (θ_i) drawing from the population mean (μ) and variance (Σ^2). (C) Bayesian-PBPK analysis was used to update the prior distribution ($Pri(\theta_{i,K})$) with experimental data Y_{ij} to generate the (D) posterior distribution ($Pos(\theta_{i,K}')$) using MCMC simulations. The PBPK model f depends on measured covariate φ_i. Exposure regimen E_i relates the prior parameters θ_i to experimental data Y_{ij} for individual i ($i = 1…n$) and specific experiment j ($j = 1…n$) at the time point t_{ij}. The difference between the observed and predicted values (i.e., residual error, ε_j) has variance σ^2. (For interpretation of the references to color in this figure legend, the reader is referred to the web version of this article.)

has a high affinity to serum albumin (Beesoon and Martin, 2015), poorly eliminated (Butenhoff et al., 2012; Harada et al., 2007) and mainly accumulated in liver and plasma (Bogdanska et al., 2011; Cui et al., 2009; Seacat et al., 2002). PFOS elimination is highly variable between species. The half-lives of PFOS range from days in rats (7–82 days) (Chang et al., 2012; Kim et al., 2016) and mice (30–42 days) (Chang et al., 2012), weeks in monkeys (15–24 weeks) (Chang et al., 2012; Seacat et al., 2002) to years in humans (3.3–6.9 years) (Olsen et al., 2007; Worley et al., 2017a). This species specificity in biological half-lives of PFOS has been considered to be similar to that of the more extensively studied structurally similar compound perfluorooctanoic acid (PFOA). It has been proposed that the hormonally-mediated, saturable renal reabsorption of PFOA and PFOS via organic anion transporters (OATs) expressed on the apical and basolateral membranes of the proximal tubule cells (PTCs) plays a key role, contributing to the large variation of biological half-lives of PFOA and PFOS between species (Kudo et al., 2002; Weaver et al., 2010; Yang et al., 2010a). The role of transporter-mediated renal reabsorption in the differential retention of PFOA and PFOS across species has been supported by the earlier physiologically-motivated modeling studies (Andersen et al., 2006; Loccisano et al., 2011; Tan et al., 2008).

To aid risk assessment of PFOS and related compounds, pharmacokinetic and PBPK modeling studies for PFOA and PFOS have been conducted in humans, monkeys and rats (Andersen et al., 2006; Fabrega et al., 2015; Fabrega et al., 2014; Fabrega et al., 2016; Loccisano et al., 2011; Loccisano et al., 2012; Tan et al., 2008; Wambaugh et al., 2013; Worley and Fisher, 2015; Worley et al., 2017b). In general, these models simulate the prolonged serum half-life by including a renal reabsorption process of PFOA or PFOS from the filtrate compartment back into the systematic circulation via renal transporter proteins. In the earlier modeling studies for PFOA and PFOS, Andersen et al. and Tan et al. (Andersen et al., 2006; Tan et al., 2008) developed a physiologically-motivated model accounting for the saturable renal resorption to simulate the monkey and rat data. The main contribution from these earlier studies was to show explicitly that saturable renal reabsorption process could result in the observed dose-dependent relationship at higher doses in monkeys (i.e., clearance increased with increasing doses) and the need to include a filtrate subcompartment in the active transporters-mediated process of the kidney compartment. Subsequently, Loccisano et al. expanded their model by integrating physiologically relevant compartments to develop a PBPK model (Loccisano et al., 2011; Loccisano et al., 2012). More recently, Worley and Fisher et al. (Worley and Fisher, 2015; Worley et al., 2017b) expanded Loccisano's model (Loccisano et al., 2012) by including physiological description of both basolateral and apical membrane transports for the simulation of sex-specific kinetics of excretion and reabsorption of PFOA in kidneys. In addition, a compartmental model for PFOA and PFOS was developed by Wambaugh et al. (2013) based on the physiologically-motivated compartment model of Andersen et al. (2006) to simulate the internal dosimetry in the rat, mouse, and monkey. U.S. EPA applied Wambaugh's model to derive chronic oral reference doses (RfDs) for PFOA and PFOS (EPA, 2016a, 2016b). The compartmental model was able to describe the experimental data well, but there are some limitations and uncertainty as the model is not physiologically based and the parameters are not biologically plausible and thus are of high uncertainty (Dong et al., 2017; Wambaugh, 2018).

In order to address the above-mentioned data gaps and limitations, the objective of this study was to develop and validate a more robust PBPK model for PFOS in multiple species, including mice, rats, monkeys, and humans. Bayesian analysis with Markov chain Monte Carlo (MCMC) simulation was performed to characterize the uncertainty of parameters and to further improve the model reliability. A sensitivity analysis of the optimized model parameters was conducted to assess the impact of uncertainty/variability in model parameter values on predictions of output across species. Furthermore, model applications were performed to predict internal dosimetry of relevance to risk assessment for reducing the uncertainty of extrapolation from animals to humans in the derivation of acceptable exposure levels. All model codes and raw data are provided in the Supplemental Materials to allow to reproduce our results and facilitate the application and extrapolation of this model to other perfluoroalkyl substances.

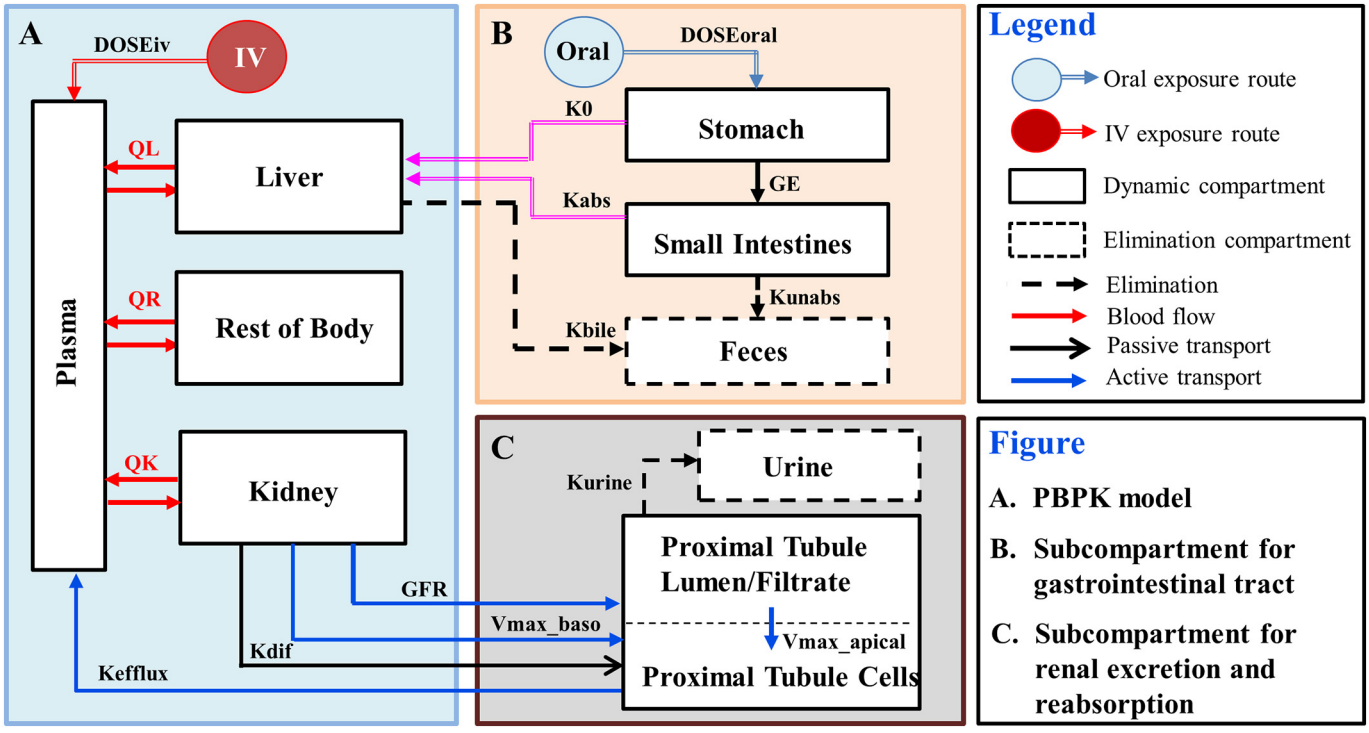

Fig. 2. Overall structure of the PBPK model for PFOS in the mouse, rat, monkey and human. The model structure was modified based on Worley and Fisher (2015) and Worley et al. (2017b). The parameter symbols were defined in Table 2. (For interpretation of the references to color in this figure legend, the reader is referred to the web version of this article.)

2. Materials and methods

2.1. Study framework

The study framework is illustrated in Fig. 1. To characterize the interspecies uncertainties and variability of model parameters, a hierarchical Bayesian approach was applied to the PFOS PBPK model across species. The basic element of this study includes: (1) the development of multiple-species PFOS PBPK model (Fig. 1A), (2) Bayesian analysis with MCMC simulation (Fig. 1B–C), and (3) evaluation of posterior parameters (Fig. 1D).

2.2. Model development and evaluation

2.2.1. PBPK model development

A consistent PBPK model structure for PFOS was used in all studied species, including the mouse, rat, monkey, and human (Fig. 2). The model structure was based on the recently published PBPK models for PFOA (Worley and Fisher, 2015; Worley et al., 2017b) to allow parallel comparisons of the simulation results for these two structurally similar compounds. In brief, the model consisted of four organ compartments (plasma, liver, kidney, and rest of the body) (Fig. 2A). A two-compartment model was used to simulate the gastrointestinal (GI) tract (stomach and small intestine) (Fig. 2B), and the kidney was described as a three-compartment model comprising of proximal tubule lumen/filtrate, PTCs, and the rest of kidney (Fig. 2C). Both intravenous (IV) and oral exposure routes were included in this model.

In the oral exposure route, PFOS enters the small intestine with a rate defined by the gastric emptying time (GE, first-order constant) after oral administration of PFOS into the stomach. Uptake in the stomach was described using a first-order rate constant (K0) while the first-order rate constant (Kabs) was used to describe the uptake of PFOS in the small intestine. PFOS absorbed in the GI tract is transported to the liver via the portal vein. IV administration of PFOS was simulated to enter directly into systematic circulation.

In the kidney compartment, PFOS enters the filtrate in the lumen of the proximal tubule from kidney blood via glomerular filtration (GFR), and subsequently is excreted to the urine via a first-order rate constant (Kurine) or actively translocated into PTCs via apical transporters described by non-linear Michaelis-Menten parameters Vmax_apical and Km_apical. PFOS is also translocated into the PTCs from kidney blood via basolateral transporters, and this process was also described using the Michaelis-Menten equation with the parameters of Vmax_baso and Km_baso. PFOS is also passively translocated into the PTCs via a diffusion rate constant (Kdif). Moreover, a previous study has suggested that a possible efflux pathway could actively transport the intracellular PFOS back into systemic circulation (Yang et al., 2010a). This model described this movement using a first-order rate constant (Kefflux). Taken together, the renal resorption pathway was simulated by the apical transporters-mediated active process (Vmax_apical and Km_apical) plus a first-order efflux process (Kefflux).

PFOS is heavily bound to plasma proteins in rats, monkeys, and humans following in vitro incubation (Kerstner-Wood et al., 2003). Only the free fraction (Free) of PFOS was assumed to be available for distribution. This was simulated using a free fraction constant (Free) that was multiplied by the total concentration of PFOS in the plasma to describe the unbound PFOS moving into and out of each compartment. Excretion of PFOS includes biliary, urinary, and fecal pathways described as a first-order elimination process in the model. The complete mathematical description is provided in Supplemental Materials.

2.2.2. Key in vivo toxicokinetic data

An extensive search of PFOS in vivo toxicokinetic (TK) datasets was performed to collect data for model calibration and evaluation. The datasets used in this study were listed in Table 1 with the indication of the exposure route (oral gavage and/or IV dosing routes), dosing regimens, matrix (plasma, urine, feces, liver and/or kidney), and species, as well as the purpose of each dataset (calibration, optimization and evaluation). All 19 PFOS TK studies in the mouse (CD-1), rat (Sprague-Dawley), monkey (Cynomolgus) and human (general population) were

Table 1
Pharmacokinetic studies in rats, mice, monkeys, and humans used for model development and evaluation.

Reference	Dose regimen	Matrix	Cal	Opt	Eva
Sprague Dawley rat					
3M unpublished data	Single oral dose at 2 mg/kg	Plasma	X		
Chang et al. (2012)	Single oral dose at 4.2 mg/kg	Plasma	X		
Johnson et al. (1979)	Single IV dose at 4.2 mg/kg	Urine	X		
Kim et al. (2016)	Single oral dose at 2 mg/kg	Plasma	X		
Kim et al. (2016)	Single IV dose at 2 mg/kg	Plasma		X	
3M unpublished data	Daily oral dose at 1 mg/kg for 4 weeks	Plasma		X	
3M unpublished data	Single oral dose at 15 mg/kg	Plasma		X	
Chang et al. (2012)	Single oral dose at 15 mg/kg	Urine		X	
Seacat et al. (2003)	Daily oral dose at 0.03, 0.13, 0.34, 1.33 mg/kg for 14 weeks	Plasma; liver			X
CD-1 mouse					
Chang et al. (2012)	Single oral dose at 20 mg/kg	Plasma; liver, kidney, urine	X		
Chang et al. (2012)	Single oral dose at 1 mg/kg	Plasma; liver, kidney, urine		X	
Cynomolgus monkey					
Chang et al. (2012)	Single IV dose at 2 mg/kg	Urine, plasma	X		
Seacat et al. (2002)	Daily oral dose at 0.03, 0.15 and 0.75 mg/kg for 26 weeks	Plasma		X	
Seacat et al. (2002)	Daily oral dose at 0.03, 0.15 and 0.75 mg/kg for 26 weeks	Liver			X
Human: general population					
Haug et al. (2009)	Unknown	Plasma	X	X	
Fabrega et al. (2014)	Unknown	Plasma; liver, kidney			X
Olsen et al. (2003a)	Unknown	Plasma			X
Olsen et al. (2003b)	Unknown	Liver			X
Olsen et al. (2008)	Unknown	Plasma			X

Note: All graphic pharmacokinetic data were extracted from selected studies using WebPlotDigitizer (version 4.10, https://automeris.io/WebPlotDigitizer/; last accessed December 28, 2018.). The 3M unpublished data were extracted from the Loccisano et al. (2012). Cal: Calibration; Opt: Optimized by MCMC algorithm; Eva: Evaluation.

used for model development and evaluation (Table 1). Only data in males were considered in this study due to the possible gender difference in the TK properties of PFOS (Kim et al., 2016; Li et al., 2017b). The present model serves as a foundation to extrapolate to females, which is a subject of our future studies. Additional details describing the data sets are provided in the Supplementary materials.

2.2.3. Preliminary model calibration

To provide prior distributions for the model parameters and to improve the performance of the model optimization using the Markov chain Monte Carlo (MCMC) algorithm, preliminary model calibration for the PBPK model was performed. Prior to the calibration analysis, a local sensitivity analysis was conducted for all selected model parameters using R package FME (Soetaert and Petzoldt, 2010) to identify sensitive parameters in the model. The initial model parameter values including physiological parameters (Table S1a) and chemical-specific parameters (Table S1b) were from the previous PBPK models for PFOA or PFOS in mice, rats, monkeys, and humans. Then, the sensitive parameters, as shown in Table S2a, were estimated using the Levenberg–Marquardt algorithm based on available in vivo calibration datasets for each species (Table 2). The estimated parameters for each species were presented in Table 2 as the prior information for inclusion in the subsequent parameter optimization using the Bayesian MCMC method. All species-specific physiological parameters were adapted from the literature and listed in Table 2.

2.3. Bayesian approach to optimize the PBPK model parameters

A reported hierarchical Bayesian approach (Bois, 2000; Bois et al., 1996; Gelman et al., 1996) was used to characterize the uncertainty and variability of model parameters in the present PFOS PBPK model for each species. This method has been extensively applied in the characterization of PBPK model parameters (Chiu et al., 2014; Chiu and Ginsberg, 2011; Chiu et al., 2009; Hack et al., 2006). In the hierarchical structure (as illustrated in Fig. 1), the analysis was composed of different levels, including the population level, individual level (i), and study level (j). The population level contained hyperprior distributions for the population mean (μ) and variance (Σ^2) for each of the selected parameters, reflecting the population variability and uncertainty of individual values. At the subject level, each model parameter (θ) is drawing by random sampling from the population mean (μ) and variance (Σ^2) (Fig. 1A and B). The predicted value of experimental data (j), for each subject i, is determined by a model function f (i.e. the PBPK model) of exposure regimen (E), dosing time (t), a set of model parameters (θ) and fixed parameters (φ) (e.g., body weight, tissue volume): $f_{ij}(\theta_i, \varphi_i, E_{ij}, t_i)$. The specification of the conditional dependencies among the population and subject parameters link the model f to the data (y) and unknown error (ε) (Fig. 1C). The unknown ε error that represents the measurement or model error was assumed to be independent and log-normally distributed with mean of zero and variance σ^2.

The focus of this study was to characterize the uncertainty and variability of key and unmeasured/unknown parameters across species and its related parameters, rather than estimating every possible model parameter. Thus, only highly sensitive model parameters were considered in the Bayesian analysis. Physiological parameters, such as the body weight, tissue volumes, and plasma flow rates were obtained from the literature and were fixed in the Bayesian analysis.

2.3.1. Assignment of prior parameter distributions

As described above, the prior distribution for the population mean (μ) was specified based on the hyperparameter mean value (M) and the variance (S^2). The M value for each model parameter was taken from the literature or estimated from the preliminary model calibration (Table 2). All prior parameters were defined with a log-normal distribution and the log-transformed parameters were described with a truncated normal distribution (2.5%–97.5%). The distribution for the population mean (μ) was truncated to include 95% of the distribution (mean ± 1.96 SD for a normal distribution) to avoid sampling from implausible values. Depending on the uncertainty of parameters, the S value of each parameter was assumed to be the value of 50% for the coefficient of variance (CV) in the model (Hack et al., 2006).

Prior distribution for the population variances (Σ^2) were defined using inverse gamma distributions: $\Gamma^{-1}(\alpha,\beta)$, where α is the shape parameter ($\alpha > 0$) and β is the inverse scale parameter ($\beta > 0$). The value of α is equal to 3 based on the assumption of 100% coefficient of uncertainty (CU), and β is set to equal to $(\alpha - 1)\cdot\Sigma_0^2$ (Hack et al.,

Table 2
Values of the species-specific parameters after model calibration for the mouse, rat, monkey and human.

Parameters	Symbol	Mouse	Rat	Monkey	Human
Body weight, (Kg)[a]	BW	0.025	0.3	3.5	82.3
Cardia output, (L/h/kg$^{0.75}$)[b]	QCC	16.5	14	18.96	12.5
Fractional blood flows (% QC)[b]					
Liver	QLC	0.161	0.183	0.194	0.250
Kidney	QKC	0.091	0.141	0.123	0.175
Fractional volumes (% BW)[b]					
Liver	VLC	0.055	0.035	0.026	0.026
Kidney	VKC	0.017	0.0084	0.004	0.004
Plasma	VPlasC	0.049	0.0312	0.0448	0.0428
Filtrate[c]	VfilC	0.0017	0.00084	0.0004	0.0004
Volume of PTCs, (L/g kidney)[c]	VPTCC	1.35e-4	1.35e-4	1.35e-4	1.35e-4
Amount of proteins in PTCs[d] (mg/cell)	Protein	2.0e-6	2.0e-6	2.0e-6	2.0e-6
Hematocrit[e]	Htc	0.48	0.46	0.42	0.44
Partition coefficients[f]					
Liver	PL	7.65*	3.66*	3.72	2.03*
Kidney	PK	0.8	0.8	0.8	1.26
Rest	PRest	0.23*	0.26*	0.15*	0.2
Free fraction of PFOS in plasma[g]	Free	0.02*	0.09	0.016*	0.014*
Glomerular filtration rate constant, (L/h/kg of kidney)[h]	GFRC	59	62.1	21.85	24.19
Gastric emptying rate constant, (/h/kg BW$^{0.25}$)[i]	GEC	0.54	0.54	2.34	3.51
Transporter rates[j]					
Vmax of basolateral (pmol/mg protein/min)	Vmax_baso_invitro	393.45	393.45	439.2	479*
Km of basolateral (mg/L)	Km_baso	27.2	27.2	20.1	20.1
Vmax of apical (pmol/mg protein/min)	Vmax_apical_invitro	4185*	1808*	76972*	51803*
Km of apical transporters (mg/L)	Km_api	52.3	278*	45.2*	64.4*
Relative activity factor[j]					
Apical transporters (unitless)	RAF_api	2.81*	1.90*	0.0014*	0.001*
Basolateral transporters (unitless)	RAF_baso	3.99	4.15*	1	1
Other rate constants (/h/kg BW$^{0.25}$)[j]					
Uptake from stomach to liver,	K0C	1	1	1	1
Absorption from small intestines to liver	KabsC	1.10*	2.12	2.12	2.12
Unabsorbed dose to appear in feces	KunabsC	7.05e-5	7.05e-5	7.05e-5	7.05e-5
Rate of efflux of PFOS from PTCs into blood	KeffluxC	5.60*	2.09*	0.1	0.15*
Diffusion rate from PTCs	Kdif	4.6e-5*	5.1e-4*	0.001	0.001
Biliary elimination rate	KbileC	3.9e-4*	0.0026*	7.8e-4*	1.3e-4*
Urinary elimination rate	KurineC	1.60	1.60	0.092*	0.096*

* Calibrated values were fitted (the initiate values are provided in Table S1) with experiment data using the Levenberg-Marquardt algorithm.
[a] Use measured value if available, or collected from Brown et al. (1997) for rodents and monkeys and from ICRP (2002) for humans.
[b] The baseline value was obtained from Brown et al. (1997).
[c] The baseline value was assumed to be 10% kidney volume based on Worley and Fisher (2015) and Worley et al. (2017b).
[d] The baseline value was obtained from Addis et al. (1936) and Hsu et al. (2014).
[e] The baseline value was obtained from Hejtmancik et al. (2002) (mouse); Davies and Morris (1993) (Rat); Choi et al. (2016) (Monkey); ICRP (2002) (human).
[f] Loccisano et al. (2012) (mouse and rat) and Loccisano et al. (2011) (monkey); Fabrega et al. (2014) (human).
[g] The baseline values were obtained from Loccisano et al. (2012) (mouse and rat) and Loccisano et al. (2011) (monkey and human).
[h] Qi et al. (2004) (mouse), Corley et al. (2005) (rat and human), Iwama et al. (2014) (monkey).
[i] Yang et al. (2015) (mouse, rat and human), Fisher et al. (2011) (monkey).
[j] Initiate values were assumed to be equal to those of PFOA adopted from Worley and Fisher (2015) (rat and mouse) and Worley et al. (2017b) (human and monkey), and then were re-estimated in the present model.

2006). The $\Sigma_0{}^2$ is the central value of population variance (Σ^2), and most parameters was set to 30% to represent the moderate level of variations. Due to possible high uncertainty existed in unmeasured parameters such as Vmax and Km of basolateral/apical transporters in PTCs, a 50% of CV was assigned to these parameters. In addition, the prior distribution of unknown error (σ^2) was modeled as a log-uniform distribution at the central value of 0.5 with the boundary of 0.01 and 3.3 for all measurements (Covington et al., 2007; Hack et al., 2006).

2.3.2. Bayesian-MCMC simulation

From Bayes' theorem, the joint posterior distribution of the parameter $p(\theta, \mu, \Sigma^2, \sigma^2|y)$ is proportional to the likelihood of data multiplied by the prior distribution. Then, the posterior distribution updated by incorporation of new data was written as:

$$p(\theta, \mu, \Sigma^2, \sigma^2 \mid y, \varphi, E, t)$$

$$\propto p(y|\ \theta, \sigma^2, \varphi, E, t) \bullet p(\theta|\ \mu, \Sigma^2) \bullet p(\mu) \bullet p(\Sigma^2) \bullet p(\sigma^2)$$

where the $p(y|\theta, \sigma^2, \varphi, E, t)$ is the likelihood of data term, which is written as $\log(y) \sim N(logf(\theta, \varphi, E, t), \sigma^2)$ by normal measurement model. At the subject level, the PFOS concentration at time point t was predicted by the PBPK model f based on a set of prior parameters (θ, φ, E, t) with an independent variance σ^2, which is related to the observed data y. Similarly, the joint prior parameters were written by normal measurement model. As described above, the joint probability of θ: $p(\theta|\mu, \Sigma^2)$ was specified by truncated normal measurement model, which was written as $\log(\theta_i) \sim N(\mu, \Sigma^2)$. Each probability of μ and Σ^2: $p(\mu)$, $p(\Sigma^2)$ is assigned with an independent hyperprior distribution as: $\log(\mu) \sim N(M, S^2)$, and population variances (Σ^2): $\Gamma^{-1}(3, 2\Sigma_0{}^2)$. The probability of unknown error $p(\sigma^2)$ is assigned as a log-uniform prior distribution with the bounds of 0.01 and 3.3 for all measurements as used in previous models (Chiu et al., 2014; Chiu et al., 2009).

Given the distribution assumption listed above, the posterior parameters can be numerically evaluated. The Delayed Rejection Adaptive Metropolis (DRAM) sampling was used to update parameters (Haario et al., 2006). Four Markov chains of 500,000 iterations each, for the rat, mouse, monkey and human models, respectively, were run with the first 250,000 iterations as "burn-in" iterations (i.e. iterations for which the simulation had not converged yet) and the last 50,000 iterations

were used as output iterations to check convergences.

All model simulations were conducted using R language (version 3.5.2, 2018; R Development Core Team, http://www.R-project.org). The PBPK model was coded in R package "mrgsolve". MCMC simulations were performed in the R software package "FME", which was developed particularly for the non-linear model and MCMC simulations. All model codes are open-source and available in the Supplementary Materials and in GitHub (https://github.com/KSUICCM/PFOS). Additionally, the model codes will be available on our website (https://iccm.k-state.edu/) upon publication.

2.4. Estimation of posterior distributions

2.4.1. Convergence

Using the MCMC sampling algorithm, each chain should be inspected to verify that equilibrium has been achieved. The convergences of the posterior parameter distributions sampled from the MCMC simulation were diagnosed by the potential scale reduction factor ($\hat{R}$) (Gelman et al., 1996) and Brooks-Gelman multivariate shrink factor (MPSRF). When each MCMC independent chain moves together and towards to the common distribution, the $\hat{R}$ ratio is decreased to the unity. A convergence diagnostic $\hat{R}$ value of 1.2 or less has been proposed as a criterion of acceptable convergence (Gelman et al., 2004).

2.4.2. Comparisons of model predictions with calibration datasets

The posterior parameter distributions at population levels were used to generate a global evaluation of model fit between log-transformed values of observed and predicted plasma and tissue concentrations, and the determination coefficient (R^2) was calculated. The optimized posterior parameters were used to predict PFOS concentrations, and then to compare the predicted values with the experimentally observed values. The predicted-to-observed ratio for each calibrated and optimization dataset was used to estimate whether the model predictions within an acceptable level of correspondence with the experimental data. Based on the acceptance criteria from World Health Organization (WHO) (WHO, 2010), estimated predicted-to-observed ratio within a factor of 2 (i.e. the ratio is within < 2 and > 0.5) indicates acceptable prediction result.

2.4.3. Model evaluation: Validation and sensitivity analysis

The optimized model with the posterior parameters was used to generate the population simulations of PFOS levels in plasma and other organs and then the simulated results were compared with the independent datasets that have not been used in the model calibration or optimization. The distributions of posterior parameters were computed with 5000 parameters vectors drawn from every 10th vector of the final 50,000 MCMC runs. Time-course simulations of PFOS concentrations were extracted for the median output with 95% confidence interval (CI) of the population simulations, and the simulated results were compared with the independent datasets in rats, monkeys and humans listed in Table 1. A detailed description on different exposure paradigms for rats, monkeys, and humans used in the model evaluation is provided in the Supplementary Materials (Section 4: Model evaluation). Due to limited mouse data, all available mouse data were used for model calibration and optimization. Thus, there were no independent mouse data for model evaluation.

A local sensitivity analysis was performed to determine which posterior parameters were most influential on the area under the curve (AUC) of plasma, liver and kidney concentrations of PFOS in the mouse (single oral dose to 1 mg/kg/day), rat (daily dosing to 1 mg/kg/day for 98 days) (Seacat et al., 2003), monkey (daily dosing to 0.75 mg/kg/day for 182 days) (Seacat et al., 2002) and human (daily dosing to 4.5 ng/kg/day for 25 years) (Haug et al., 2009). Each of the posterior parameters was increased by 1%, and the corresponding AUCs of PFOS concentrations were computed. Normalized sensitivity coefficient (NSC) was calculated using Eq. (S13) (Lin et al., 2011; Mirfazaelian et al., 2006) provided in Supplementary Materials. The relative influence of each parameter on the response variables was categorized as: low: $|NSC| < 20\%$; medium: $20\% \leq |NSC| < 50\%$; high: $50\% \leq |NSC|$ (Lin et al., 2013; Yoon et al., 2009).

2.5. Model application to predict the human equivalent dose (HED)

The validated PBPK model was used to simulate the exposure of rats and monkeys to reported no-observed-adverse-effect-level (NOAEL) of 0.34 and 0.15 mg/kg/day, respectively (EPA, 2016b). These NOAEL values were obtained from the studies by Seacat et al. (2003; 2002), where histopathological lesions of the liver, increased liver weight and other critical toxicity endpoints related to liver were observed in rats (1.33–1.56 mg/kg/day after 14 weeks) and monkey (0.75 mg/kg/day after 26 weeks). In line with our model design, only NOAEL values derived from male rat and monkey data (Seacat et al., 2003; Seacat et al., 2002) were selected as the point of departure (POD) to derive the human equivalent dose (HED) for PFOS using the present PBPK model and then compare to the published HED values by U.S. EPA (EPA, 2016b). To calculate HED, we firstly predicted the plasma AUC at the NOAEL exposure levels for the monkey, rat and human. Because of the consideration of liver toxicity, the HED value based on the liver dosemetric was also estimated. The AUC values were calculated using the PBPK model for the duration of exposure in the selected rat and monkey critical studies or for 25 years until steady state had been achieved in humans. Subsequently, the average serum concentration (ASC) and average liver concentration (ALC) was estimated using the equation (i.e., ASC or ALC [mg/L] = AUC [mg * h/L]/(Exposure duration [days] * 24 h/1 day)) based on U.S. EPA report (EPA, 2016b). Next, HED was calculated using NOAEL multiplied by the ratio of ASC or ALC between animals and humans (e.g., ASC_{animal}/ASC_{human}) (Andersen et al., 2002; Andersen et al., 1999; Cheng et al., 2018; EFSA, 2015; Lin et al., 2016). Based on each posterior parameter combination, the median and the 95% confidence interval (CI) for ASC, ALC, and HED values were estimated and compared with the reported HED values from U.S. EPA (EPA, 2016b).

3. Results

3.1. Convergence analysis

Figs. S1–S8 (Supplementary Materials) showed the well-mixed Markov chains trace plots, suggesting well convergences among chains for each species. Corrected Scale Reduction Factors ($\hat{R}$) were calculated for the four chains based on the method of Brooks and Gelman (Brooks and Roberts, 1998). All the $\hat{R}$ values for population parameters in four species were below 1.2, indicating convergences; and the ranges of the $\hat{R}$ values were 1.0–1.01 in mice, 1.0–1.02 in rats, 1.0–1.04 in monkeys and 1.0–1.02 in humans (Figs. S1–S8). The diagnosed values of the convergences for Markov chains indicate the equilibrium posterior parameter distribution was achieved for subsequent population and individual simulations.

3.2. Estimation of posterior parameter distributions between species

The prior and posterior distributions of the median with 95% CI for the estimated parameters were shown in Table 3. The posterior distribution of population mean (μ) was estimated from the updated the central value (M) and standard deviation (S) using the MCMC simulation. The medians of posterior distributions for most parameters were close to prior estimates (defined by ± 20% from the prior estimates) (Yang et al., 2010b), but most of the 95% CIs of posterior distributions were substantially narrower than prior distributions (i.e. less uncertainty). In the Fig. 3, the posterior parameter uncertainty distributions were compared across species. Variabilities of parameter distributions between species for KeffluxC, KurineC, RAFapi and

Table 3
Median values (2.5%, 97.5%) of prior and posterior distributions for the estimated parameters in the MCMC analysis for the mouse, rat, monkey and human.

Symbol	Mouse		Rat		Monkey		Human	
	Prior	Posterior	Prior	Posterior	Prior	Posterior	Prior	Posterior
Free	0.02 (0.0004, 0.04)	0.02 (0.005, 0.03)	0.09 (0.004, 0.17)	0.02 (0.001, 0.14)	0.017 (0.0008, 0.033)	0.01 (0.0004, 0.03)	0.01 (0.0003, 0.03)	0.01 (0.0005, 0.02)
PL	3.72 (0.07, 7.36)	3.3 (2.1, 5.3)	3.66 (0.09, 7.25)	2.9 (1.7, 6.4)	3.72 (0.04, 7.36)	4.45 (1.8, 7.0)	2.02 (0.04, 4.01)	1.82 (0.06, 3.72)
PK	0.8 (0.02, 1.58)	0.2 (0.1, 0.3)	0.8 (0.02, 1.58)	0.5 (0.02, 1.4)	0.80 (0.02, 1.58)	0.5 (0.02, 1.33)	1.26 (0.02, 2.49)	0.77 (0.03, 2.10)
PRest	0.2 (0.004, 0.4)	0.2 (0.03, 0.3)	0.26 (0.004, 0.52)	0.4 (0.28, 0.51)	0.15 (0.004, 0.31)	0.2 (0.1, 0.30)	0.20 (0.004, 0.39)	0.17 (0.07, 0.31)
Vmax_baso_invitro	393 (7.89, 779)	217 (10.5, 645)	393 (2.36, 779)	244 (11.2, 634)	439 (8.79, 869)	434 (31, 797)	479 (9.59, 948)	266 (12.4, 789)
Km_baso	27.2 (0.54, 53.8)	1.1 (0.05, 3.02)	27.2 (0.39, 53.8)	15 (0.83, 45)	20 (0.4, 39.7)	1.7 (0.4, 29.8)	20 (0.4, 39)	13 (0.6, 34)
Vmax_api_invitro	4.2e3 (8.3e1, 8.3e3)	9.0e2 (4e1, 2.3e3)	1.8e3 (5.5e1, 3.6e3)	1.1e3 (5.9e1, 3.1e3)	7.7e4 (7.4e2, 1.5e5)	3.6e4 (2.5e3, 1.2e5)	5.2e4 (1.03e3, 1.02e5)	2.6e4 (1.5e3, 8.2e4)
Km_api	52.3 (1.04, 103)	25.8 (1.2, 82.5)	278 (2.99, 551)	122 (6.95, 463)	45.2 (1.5, 89.6)	28 (1.2, 75)	64 (1.28, 127)	47 (2.6, 109)
RAF_api	2.81 (0.06, 5.57)	3.7 (2.7, 6.8)	1.90 (0.04, 3.77)	1.17 (0.05, 3.17)	1.4e-3 (1e-3, 1.8e-2)	5e-4 (1e-3, 2e-2)	1e-3 (2.0e-5, 1.9e-3)	5.1e-4 (2.9e-5, 1.6e-3)
RAF_baso	3.99 (0.07, 7.90)	2.17 (0.1, 6.5)	4.14 (0.05, 8.21)	2.48 (0.12, 6.90)	1.00 (0.3, 1.9)	1.00 (0.04, 1.8)	1.00 (0.02, 1.97)	0.62 (0.02, 1.68)
K0C	1 (0.02, 1.98)	0.7 (0.03, 1.7)	1 (0.02, 1.97)	0.72 (0.03, 1.71)	1.00 (0.02, 1.97)	0.6 (0.03–1.66)	1.00 (0.02, 1.97)	0.62 (0.03, 1.67)
KabsC	1.10 (0.02, 2.19)	1.7 (0.1, 4.3)	2.12 (0.02, 4.19)	1.55 (0.19, 3.66)	2.12 (0.04, 4.19)	1.3 (0.06, 3.5)	2.12 (0.04, 4.19)	1.35 (0.06, 3.56)
KunabsC	7e-5 (1.4e-6, 1.4e-4)	7e-5 (1e-5, 3.2e-5)	7e-5 (1.2e-5, 1.4e-4)	4e-5 (2e-6, 1e-4)	7.0e-5 (1.4e-6, 1.4e-4)	4e-05 (2e-6, 1.2e-4)	7.1e-5 (1.4e-6, 1.4e-4)	4.3e-5 (2.2e-6, 1.2e-4)
KeffluxC	5.60 (0.1, 11)	1.4 (6.7e-2, 4.09)	2.09 (0.04, 4.15)	1.2 (0.05, 3.5)	0.10 (0.001, 0.19)	2.7e-2 (2e-3, 1.6e-1)	0.14 (0.003, 0.29)	0.1 (0.01, 0.25)
Kdif	4.6e-5 (9.2e-7, 9.3e-5)	6e-4 (3e-5, 1.7e-3)	5e-4 (3.8e-5, 1.0e-3)	3e-4 (1e-5, 8e-4)	1.0e-3 (2e-5, 2e-3)	2e-4 (7e-5, 7e-4)	1e-3 (2.0e-5, 2e-3)	6e-4 (2.7e-5, 1.7e-3)
KbileC	4e-4 (7.9e-6, 7.8e-4)	5e-4 (4e-4, 7e-4)	3e-3 (1.2e-5, 5.3e-3)	3e-3 (1e-3, 5e-3)	7.9e-4 (2e-5, 1.5e-3)	4e-4 (1.9e-4, 1.0e-3)	1.3e-4 (3e-6, 3e-4)	1.2e-4 (4.7e-6, 2.4e-4)
KurineC	1.60 (0.03, 3.17)	0.8 (0.04, 2.5)	1.60 (0.04, 3.16)	0.7 (0.04, 2.58)	0.09 (0.001, 0.18)	0.05 (0.003, 0.16)	0.09 (0.002, 0.19)	0.07 (0.003, 0.16)

Vmax_apical_invitro were apparent. In particular, the values of these parameters in the human and monkey were significantly different from those for rodents. Parameters that had similar posterior distributions between species included partition coefficients (PL and PK), the Michaelis-Menten parameters for basolateral membrane transporters (Vmax_baso_invitro, Km_baso), and some rate constants (K0C, KabsC, Kdif).

3.3. Comparisons of model predictions with experimental data

3.3.1. Global evaluation of model fit

A global evaluation of the goodness of fit between model predictions and experimental data across species is shown in Fig. 4A. The distributions of the predicted-to-observed ratio for each of the experimental data point are illustrated in Fig. 4B. Overall, the model predictions correlated with the majority of the experimentally measured data very well (high goodness of fit, $R^2 = 0.96$) (Fig. 4A). This model, however, underestimated some data points in the mouse and monkey datasets from Chang et al. (2012) at low dose levels with the predicted-to-observed ratio lower than 0.5 (Fig. 4B). The histogram in Fig. 4B showed that most of the predicted values were within the predicted-to-observed ratio of 2, which meets the WHO model precision criteria (WHO, 2010). All comparisons of predicted time-dependent PFOS concentration profiles with calibration and optimization data of the mouse, rat, monkey and human are shown in Supplemental Materials (Figs. S9–S12).

3.3.2. Model evaluation with independent datasets

Comparisons of measured vs. model-predicted ranges (median, interquartile and 95% CI) of PFOS concentrations in the plasma and tissues in rats, monkeys, and humans are shown in Fig. 5. For the human model, the model predictions (Fig. 5A1–A3) were compared with the measured PFOS concentrations in plasma (Fig. 5A1) from Red Cross adult donors in six cities around the U.S. in 2000–2001 (Olsen et al., 2003a) and 2006 (Olsen et al., 2008), and the exposure of 0.0045 μg/kg/day before 2000 (simulation time from 0 to 50 years in the plot; assumed that exposure from the 1950s to 2000) and 0.0018 μg/kg/day from 2001 to 2006 (simulation time from 51 to 56 years in the plot) were used in this model based on the previously reported estimated human exposures (Loccisano et al., 2011). The liver PFOS concentrations (Fig. 5A2) were collected from International Institute for the Advancement of Medicine (Olsen et al., 2003b), and only the male data ($n = 16$, age range 5–74) were considered in this model. The predicted PFOS values in plasma (Fig. 5A1) and liver (Fig. 5A2) was shown to be close to the observed values. In addition, in Fig. 5A3, the simulation results were compared with the measured PFOS concentrations in plasma, liver and kidney from an autopsy (Fabrega et al., 2014). The model-predicted steady-state concentrations of PFOS in plasma, liver, and kidney agreed with the measured concentrations in humans except for the kidney. The reasons for the underestimation of the PFOS concentrations in the kidney from the study by Fabrega et al. (2014) are unknown, but it could be due to the high uncertainty and variability of the human data, especially for different human subpopulations with different demographic, exposure, and toxicokinetic properties.

For the rat model, the experimental data were from a dietary exposure study where rats were exposed to 0.5 (0.03 mg/kg/day), 2 (0.13 mg/kg/day), 5 (0.34 mg/kg/day), or 20 (1.33 mg/kg/day) ppm of PFOS for 4 and 14 weeks, and PFOS levels in plasma and liver were determined after treatment (Seacat et al., 2003). Fig. 5B1–B2 showed the comparisons of model predictions and measured PFOS concentrations in plasma (Fig. 5B1) and liver (Fig. 5B2) on the days of 28 and 98 of the 1.33 mg/kg/day dietary exposure study. The model somewhat overestimated the plasma (Fig. 5B1) PFOS concentrations on day 28, but well predicted PFOS concentrations at the end of day 98 in plasma and liver. The model-predicted ranges of PFOS concentrations in plasma and liver well corresponded to the observed data at all dose

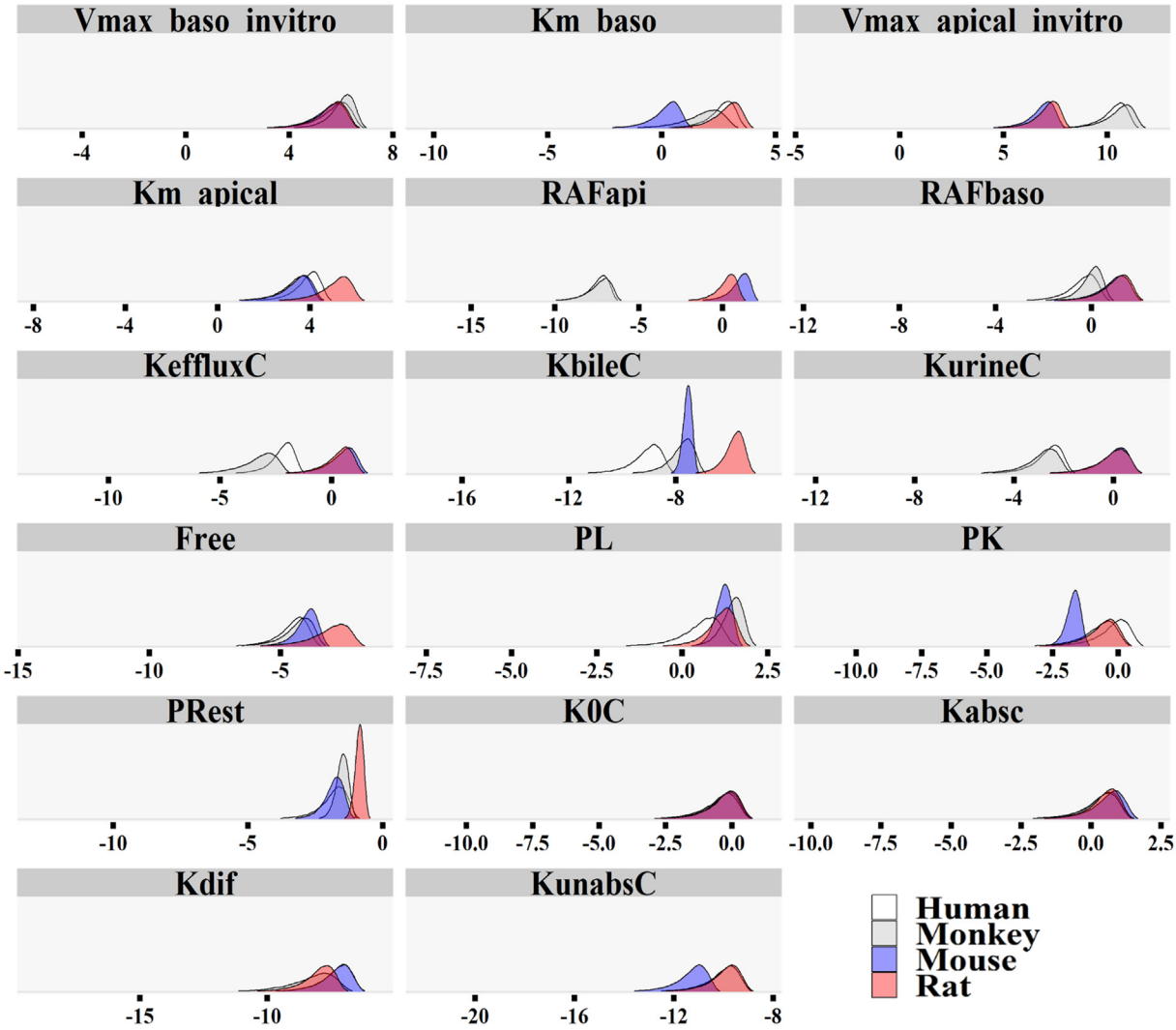

Fig. 3. Densities of posterior parameter uncertainty distributions in the mouse (blue color), rat (pink color), monkey (grey color), and human (white color) of the population mean (μ). The x-axis represents the log-transformed value of each parameter. The y-axis represents the densities of the posterior parameter uncertainty distributions. Please refer to Table 2 for definitions of parameters. (For interpretation of the references to color in this figure legend, the reader is referred to the web version of this article.)

levels (Fig. 5B3).

For the monkey model, comparisons of model-predicted vs. measured PFOS concentrations in liver resulting from an oral dose of 0.03, 0.15, and 0.75 mg/kg daily to monkeys (Seacat et al., 2002) are shown in Fig. 5C1–C2. The predicted time-course PFOS concentrations were slightly higher than the measured PFOS concentrations in liver (Fig. 5C1) at 0.75 mg/kg and other dose groups (Fig. 5C2) at the end of day 182. Overall, the present model was able to simulate the majority of available independent data with acceptable accuracies, indicating model validation across rats, monkeys, and humans.

3.4. Posterior parameter sensitivity

A local sensitivity analysis was carried out for a total of 68 posterior parameters based on the PBPK model for the mouse, rat, monkey, and human, respectively. Results of the local sensitivity analysis based on 1% variation of the posterior parameter values in the simulation of plasma, liver and kidney are shown in Fig. 6. The results indicate that there appears to be a species-specific difference in model sensitivity to parameters. Serum PFOS is primarily dependent on the parameters Free, PL and K_{bileC} in the mouse and rat. In the monkey and human, besides Free, PL and K_{bileC}, serum PFOS AUC is also governed by the parameters related to membrane transporters such as V_{max_apical}, K_{m_apical}, RAF_{api}, RAF_{baso} (Fig. 6A). Moreover, there was a significant tissue-specific difference in parameter sensitivity (Fig. 6A–C). In humans, the AUC of the plasma and liver are highly sensitive to Free, PL and the parameters related to apical transporters (Vmax_apical_invitro, Km_apical), whereas the parameters related to basolateral transporters (Vmax_baso_invitro, Km_baso, RAFbaso) had the highest sensitivity on the AUC of kidney.

3.5. Model application to predict the human equivalent doses (HEDs)

The result of the comparison of the HED values from the current US EPA document (EPA, 2016b) with those HED values resulting from the use of our PBPK model is shown in Table 4. The estimated ASC ranged from 0.015 to 1.30 (median: 0.56) μg/mL and from 0.034 to 2.77 (median: 0.46) μg/mL on the basis of the NOAEL in monkey (Seacat et al., 2002) and rat studies (Seacat et al., 2003), respectively, which were about 68-fold and 36-fold lower than the U.S. EPA guideline values of ASC for monkeys and rats, respectively. The estimated ALC ranged from 80 to 288 μg/mL and 33 to 125 μg/mL resulting from monkey and rat studies, respectively. The PBPK model-derived plasma dosimetry-based HED levels was 0.0055 (95% CI: 0.0001–0.14) and

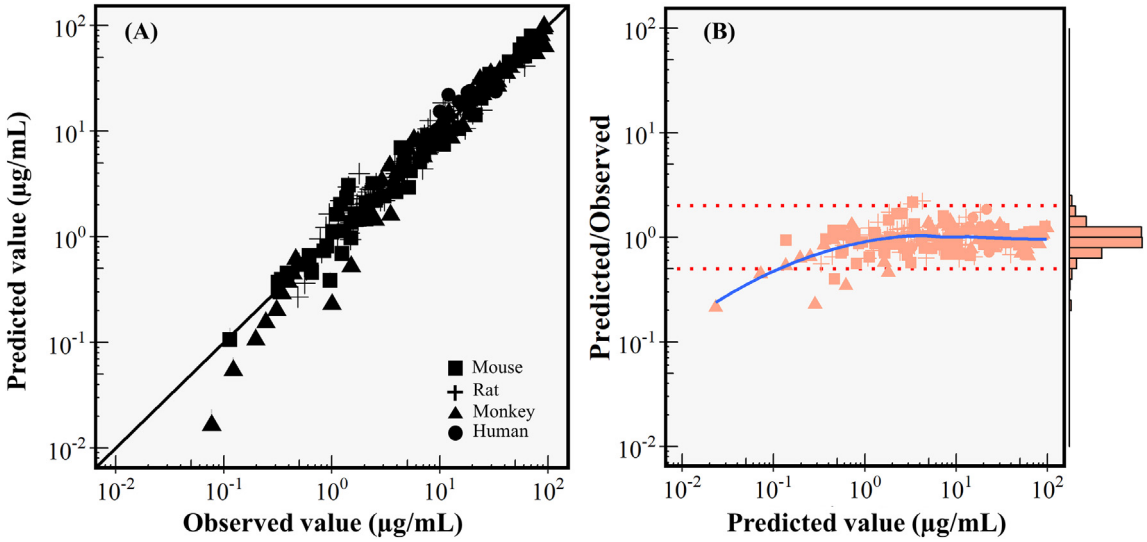

Fig. 4. Comparisons of model predictions (y-axis) with observed data (x-axis) with (A) global evaluation of goodness of model fit and (B) predicted-to-observed ratio versus model prediction plot. In plot (A), the different symbol shapes are used for different species, including the mouse (square), rat (cross), monkey (triangle) and human (round). The solid black diagonal line represents the unity line where the observed value and the predicted value are equal. In plot (B), the dashed line represents over a predicted-to-observed ratio of 2 or lower 0.5, and the blue line is the smoothed high order polynomial curve. The histogram of residuals is shown on the right of the panel. (For interpretation of the references to color in this figure legend, the reader is referred to the web version of this article.)

0.0057 (95% CI: 0.0002–0.17) mg/kg/day based on the ASC from the monkey and rat studies, respectively; while the liver dosimetry-derived HED values were 0.012 (95% CI: 0.004–0.22) and 0.004 (0.0013–0.072) mg/kg/day, respectively.

4. Discussion

Risk assessment of PFOS is challenging due to its large variation in toxicokinetics between species and a lack of a robust PBPK model to take account toxicokinetic uncertainty across species (ATSDR, 2018; Dong et al., 2017; EPA, 2016b). In the present study, built upon earlier PBPK models for PFOS and PFOA, we developed a robust PBPK model for PFOS in multiple species, including mice, rats, monkeys, and humans. The model parameters were rigorously optimized with Bayesian analysis through MCMC simulation and the model was validated with independent data in rats, monkeys, and humans. This model greatly improves the understanding of the interspecies uncertainty/variations of toxicokinetic parameters for PFOS. The model could be used to derive HED based on NOAEL from animal toxicity studies. This multiple species-specific PBPK models with optimized parameters can potentially improve quantitative risk assessment for PFOS, and this open-source model serves as a foundation for developing PBPK models for other perfluoroalkyl substances.

4.1. Optimization, uncertainty, and variability of model parameters across species

The present PFOS PBPK model used a consistent model structure across multiple species and incorporated the Bayesian approach through MCMC simulation to optimize the parameter values and inform the interspecies uncertainty and variability of model parameters. In the optimization of model parameters, several transporter parameters that were originally obtained from human or rat cells (e.g., Vmax_apical_invitro, Km_apical, etc.) were refitted with available in vivo datasets. Despite that the posterior parameter values had a variability of 2 orders of magnitude, the median values were consistent with the baseline values observed from in vitro studies. For example, the median values of posterior distributions for Vmax_apical_invitro and Km_apical in humans were estimated to be 26,000 (pmol/mg protein/min) and 42 (mg/L), which are close (within 10×) to the average values of Vmax (2233, unit: pmol/mg protein/min) and Km (17.2, unit: mg/L) obtained from human transporters: OATP1B1, OATP1B3, and OATP2B1 in human kidney cells (HEK293) (Zhao et al., 2017). Similarly, the values of Vmax (1840, unit: pmol/mg protein/min) and Km (46, unit: mg/L) for rat transporters: OATP1A1 and OATP1A5 (Zhao et al., 2017) were consistent with our posterior values of Vmax_apical_invitro (1100, unit: pmol/mg protein/min) and Km_apical (122, unit: mg/L).

The interspecies variability was evident in the analysis of posterior parameter distributions between species (Fig. 3). Our results indicate that the posterior distributions of most chemical-specific parameters are similar between species, but apparent interspecies differences exist for the following parameters, including the urinary elimination rate constant (KurineC), resorption rate constant from PTCs into systemic circulation (Kefflux), and parameters related to apical membrane transporters (Vmax_apical_invitro and RAFapi). In particular, a 100-fold difference of posterior point estimate between the rodent and primate for KurineC has been observed, which, in part, explains the fact that the half-life in humans is much longer than in rodents (Chang et al., 2012; Olsen et al., 2008). Additionally, the finding that the posterior distributions of the renal apical membrane transporter rate and its activity factor (Vmax_apical_invitro and RAF_api) in primates are substantially different from those in rodents is consistent with the previous in vitro studies (El-Sheikh et al., 2008; Hilgendorf et al., 2007), indicating that the expression and/or activity of apical membrane transporter proteins that mediate active tubular reabsorption of PFOA and PFOS are species-specific.

Furthermore, our results suggest that the parameter simulating the process of pumping PFOS from PTCs back into the systemic circulation via the efflux pathway (Kefflux) might play a critical role in the variation of the elimination kinetics between species as the posterior distributions of Kefflux were significantly different between rodents and primates, which supports the hypothesis proposed by a recent study (Yang et al., 2010a) that the efflux transporters (e.g., multidrug resistance-associated protein 6 and organic solute transport α/β) might assist in moving intracellular perfluorocarboxylates back to the systemic circulation to extend the serum half-life. Future studies are needed to determine the specific and quantitative role of these transporters in the half-life of PFOS in different species.

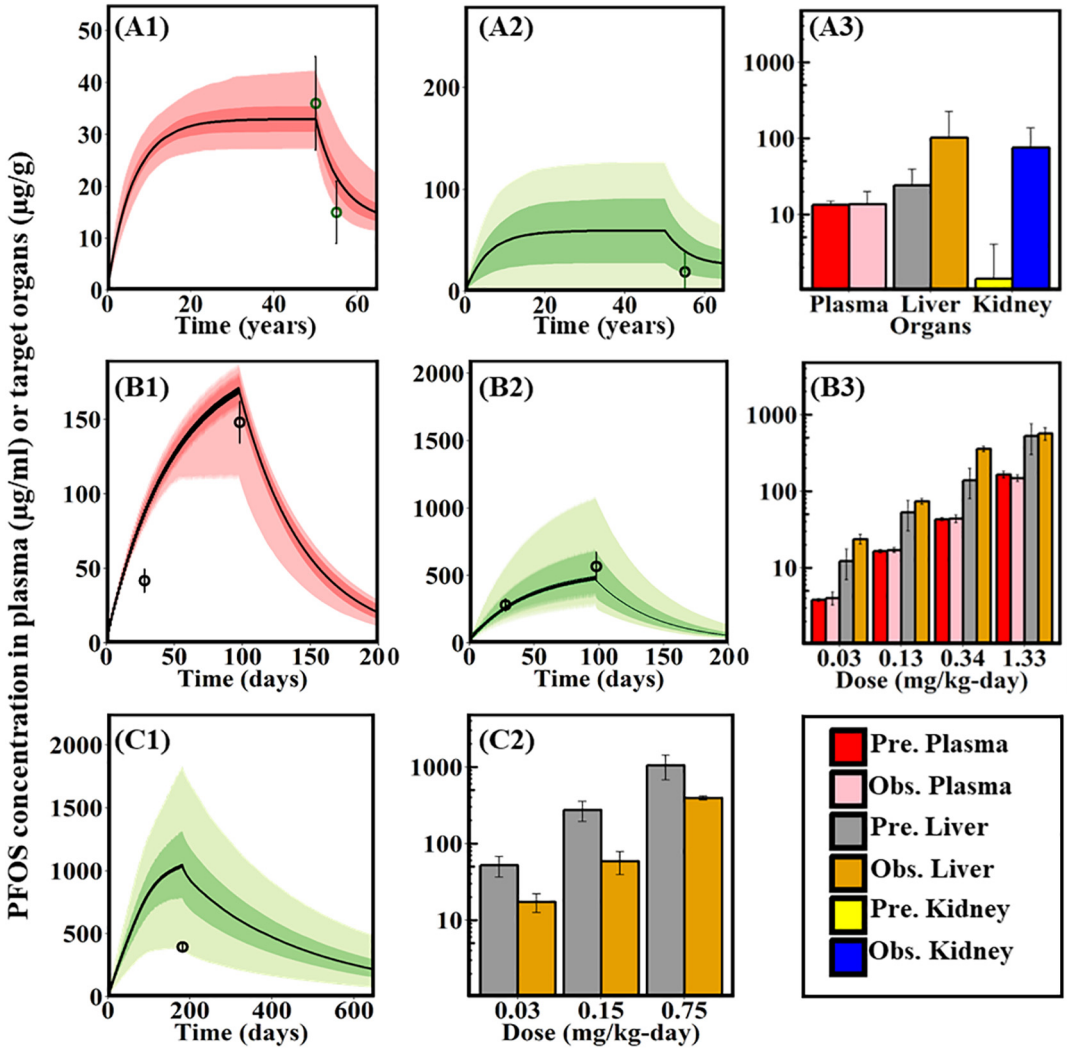

Fig. 5. Comparisons of model simulations and experimental data (mean ± SD) from studies in (A1–A3) humans, (B1–B3) rats and (C1–C2) monkeys following dietary exposure. For the human data, the serum PFOS concentrations (A1) were measured in the general population in 2000–2001 (simulation time at 50 years) (Olsen et al., 2003a) and in 2003–2006 (simulation time at 55 years) (Olsen et al., 2008), and the (A2) liver PFOS concentrations were obtained from adult donors (Olsen et al., 2003b). The PFOS concentration data in A3 were obtained from the postmortem samples in an autopsy (Fabrega et al., 2014). A more detailed description on the human exposure paradigms used in the model evaluation is available in the Supplementary Materials. In the rat study (Seacat et al., 2003), serum (B1) and liver (B2) PFOS concentrations were measured at the end of 28 and/or 98 days of oral exposure at different dose levels (0.03–1.33 mg/kg/day). In the monkey study (Seacat et al., 2002), the PFOS concentrations in liver were measured at the end of 182 days of dietary exposure to (C1) 0.75 mg/kg/day and (C2) all dose groups (0.03, 0.15 and 0.75 mg/kg/day). The light and dark color represent the interquartile range (25% - 75%) and 95% confidence interval (CI), respectively. The points with error indicate the mean (± SD) of PFOS concentrations in the serum and other target organs. (For interpretation of the references to color in this figure legend, the reader is referred to the web version of this article.)

4.2. Sensitivity analysis of posterior parameters

The sensitivity analysis results suggest that the free fraction (Free), biliary elimination rate constant (KbileC) and partition coefficient of liver (PL) had high influence on the model predictions of the plasma and target tissue concentrations in rodents, whereas in monkeys and humans, besides Free, KbileC, and PL, the membrane transporters-related parameters (Vmax_baso_invitro, Vmax_apical_invitro, RAF_api, etc.) were also highly sensitive in the model simulations. These results support the findings of earlier studies (Andersen et al., 2006; Loccisano et al., 2011) that the membrane transporters in kidney may play an important role in the disposition of PFOS as they mediate the excretion and reabsorption of xenobiotics in monkeys and humans, and thus strongly contribute to the predicted PFOS concentrations in plasma and target organs. A recent study (Fabrega et al., 2016) also reported that the free fraction and transport parameters (Tm: resorption maximum and Kt: affinity constant) were the most influential parameters based on the sensitivity analysis results, which are consistent with our findings. Moreover, the finding that the model predictions were sensitive to the values of partition coefficient of liver in rodents was not surprising as it has been shown that PFOS distributes preferentially to the liver in rodents compared with primates (Bogdanska et al., 2011).

4.3. Dosimetry and risk assessment

One of the biggest challenges in risk assessment for PFOS is the derivation of acceptable exposure levels from critical studies in animals to humans. Due to the large interspecies variation in toxicokinetics between species, similar external PFOS dosages (i.e., mg/kg/days) in animals may result in substantially different internal dosimetry in humans. In addition, there are physiological and biochemical differences among mice, rats, monkeys, and humans that have to be accounted for when conducting interspecies extrapolation. Non-biologically-based parameters from the compartmental TK model were not suitable to

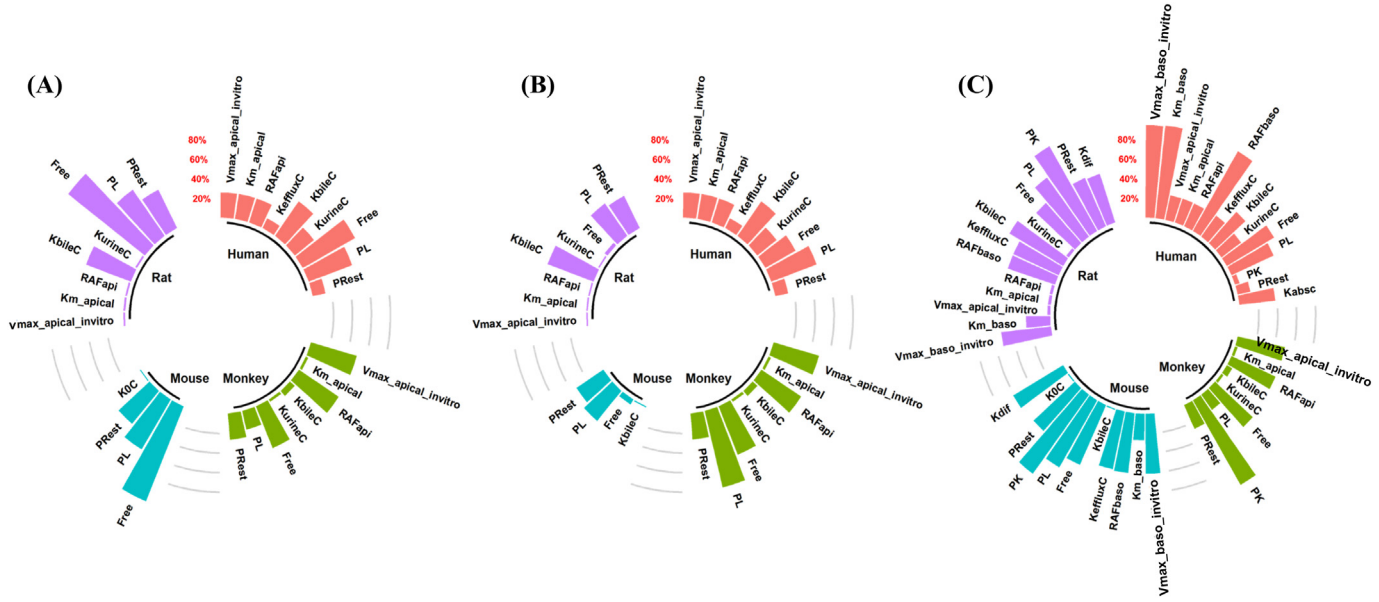

Fig. 6. Normalized sensitivity coefficients (NSCs) of posterior parameters using AUCs for concentrations of PFOS in (A) plasma, (B) liver, and (C) kidney in the mouse (single oral dose to 1 mg/kg/day), rat (daily dosing to 1 mg/kg/day for 98 days), monkey (daily dosing to 0.75 mg/kg/day for 182 days) and human (daily dosing to 4.5 ng/kg/day for 25 years). Only parameters with at least one absolute value of NSC > 1% are shown on the plots. (For interpretation of the references to color in this figure legend, the reader is referred to the web version of this article.)

describe toxicokinetic behaviors of PFOS across species. For example, the three-compartment TK model incorporating the MCMC simulation (Wambaugh et al., 2013) has been used by U.S. EPA to derive the RfD of PFOS. Despite the model in Wambaugh et al. provides insight into the risk assessment of PFOS (EPA, 2016b), there is still substantial uncertainty of model parameters across species as the model is not physiologically based and the model parameters are not biologically plausible (Dong et al., 2017).

The multiple-species PBPK model reported herein was established based on the available knowledge on the mechanisms of pharmacokinetics of PFOS and by considering the model structures of available PBPK models for PFOS and PFOA so that the current model is physiologically relevant and comparable to existing models for PFOS and PFOA. Also, the same physiologically-based model structure was calibrated with data from all four species, so that the model can be used to conduct interspecies extrapolation. With the use of Bayesian analysis and MCMC simulation in the estimation of posterior parameter distribution, the uncertainty has been significantly reduced from prior parameter distributions.

A report of Food Standards Australia New Zealand (FSANZ) (FSANZ, 2016) has pointed out that the serum concentration of PFOS predicted by the PK model used in U.S. EPA guidance appears to rapidly reach the steady-state despite the long half-life. This might affect the calculation of AUC and overestimate the value. Indeed, the estimated ASC levels derived by our PBPK model based on the general acceptable AUC method were ~50-fold lower than the U.S. EPA guideline values of ASC. However, a data-driven human clearance (0.000081 L/kg/d) was applied for the derivation of HED by U.S. EPA, resulting in the conservative guidance values of HED (0.0013–0.0031 mg/kg/day). It is very close to the estimated median values of HED (0.0055–0.0057 mg/kg/day) resulting from the ASC-derived AUC from our PBPK model based on the NOAEL of monkey (Seacat et al., 2002) and rat (Seacat et al., 2003) studies (EPA, 2016b) (Table 4). Using the estimated 5th percentile of ASC-derived HED values resulting from the NOAEL of monkey and rat studies as PODs and the uncertainty factor of 30 (a factor of 10 to account for the intraspecies variability and a factor of 3 to account for interspecies variability in pharmacodynamics), the estimated RfD values ranged from 3 ng/kg/day to 6 ng/kg/day. The RfDs resulting our PBPK model are lower than those currently recommended by the U.S. EPA (20 ng/kg/day) for developmental endpoint (Luebker et al., 2005), but are closed to the health-based guidance value of European Food Safety Authority (EFSA, tolerable daily intake of 1.8 ng/kg/day) derived from human studies based on the serum cholesterol endpoint (EFSA, 2018).

Currently, the mode of action (MOA) of PFOS-induced toxicity is not fully understood, but a growing number of studies in animals have linked PFOS exposure to liver toxicity (e.g., increased liver weight and hepatocellular hypertrophy, decreases in serum cholesterol and triglyceride levels) (Elcombe et al., 2012a; Elcombe et al., 2012b; Seacat et al., 2003; Seacat et al., 2002) and developmental effects (Butenhoff et al., 2009; Lau et al., 2003; Luebker et al., 2005; Thibodeaux et al., 2003). The leading hypothesis of PFOS-induced liver toxicity is that PFOS may interfere with mitochondrial beta-oxidation of fatty acids and subsequently affect the transcriptional activity of peroxisome proliferator-activated receptor alpha (PPARa) in liver (Martin et al., 2007; Wan et al., 2012; Wang et al., 2014). The peroxisome proliferation via activation of PPARα might be a major contributing factor to the effects of PFOS on the liver and some of the developmental effects (ATSDR, 2018).

In the U.S. EPA guidance (EPA, 2016b), the HEDs estimated from the average serum concentrations based on the liver (Seacat et al., 2003) and developmental toxicity (Butenhoff et al., 2009; Lau et al., 2003; Luebker et al., 2005) endpoints were as the potential basis for the derivation of RfD. However, based upon a consideration of the MOA, the liver toxicity or developmental effects are better explained by the internal dosimetry in target organs (e.g., liver and fetal organs). In this study, the estimation of median HED values resulting from the PBPK-predicted liver AUC was similar to that resulting from the predicted of serum AUC based on the liver toxicity endpoint (e.g., 0.0057 vs. 0.004 mg/kg/day based on the rat study). Thus, it appears that the HED derived from the serum AUC is an acceptable surrogate for the target organ dosimetry for PFOS risk assessment. Although the derivation of RfDs could vary depending on the selection of internal dosimetric in the target organs (e.g., serum or liver) and the application of uncertainty factors to data from animal or human studies, the estimated RfDs derived from our model that is linked to the likely MOA (liver toxicity endpoint) potentially provides a more physiologically relevant reference value for risk assessment of PFOS.

Table 4
Human equivalent doses (HED) derived from the rat and monkey models based on the model-predicted average serum concentrations in each species.

Study; species; critical effects	Dosing duration (days)	NOAEL (mg/kg/day)	ASC[a] or ALC[b] at NOAEL (μg/mL or mg/L)		HED (mg/kg/day)	
			EPA	This study	EPA[d]	This study[e]
Seacat et al., 2002: Monkey; (Increased liver weight; histopathology change; Decreased body weight)	182	0.15	38	ASC: 0.56 (95% CI: 0.015–1.30)[c] ALC: 182 (95% CI: 80–288)	0.0031	Plasma: 0.0055 (95% CI: 0.0001–0.14) Liver: 0.012 (95% CI: 0.004–0.22)
Seacat et al., 2003: Rat; (Increased liver weight; centrilobular hepatocytic vacuolation)	98	0.34	16.5	ASC: 0.46 (95% CI: 0.034–2.77)[c] ALC: 56 (95% CI: 33–125)	0.0013	Plasma: 0.0057 (95% CI: 0.0002–0.17) Liver: 0.004 (0.0013–0.072)

[a] ASC represents the average serum concentration at the NOAEL exposure level for each species. ASC (mg/L) = Serum-AUC (mg/L * h) ÷ (24 h/day × Exposure duration [Days]).
[b] ALC represents the average liver concentration at the NOAEL exposure level for each species. ALC (mg/L) = Liver-AUC (mg/L * h) ÷ (24 h/day x Exposure duration [Days]).
[c] Mean (95% confidence interval).
[d] HED = average serum concentration (mg/L) × CL, where CL = 0.000081 (L/kg bw/day) (EPA, 2016b).
[e] HED = NOAEL × (ASC_{animal}/ASC_{human}) or (ALC_{animal}/ALC_{human}).

4.4. Limitations

The present study has several limitations. First, due to the limited human data, we used the pooled serum data from a general Norwegian population for the human model calibration (Haug et al., 2009). Although the human model has been validated using data from other general populations (Olsen et al., 2003a; Olsen et al., 2003b; Olsen et al., 2008) and human autopsy data (Fabrega et al., 2014), the fact that all human datasets had unknown exposure conditions present a challenge in the assessment of model fit. While the exposure conditions were estimated based on available knowledge from the literature, additional human studies with known PFOS exposure conditions, once available, could be used to improve the present human model. Second, unlike the Bayesian PBPK model for trichloroethylene (Chiu and Ginsberg, 2011; Chiu et al., 2009), our model fixed the physiological parameters during the MCMC optimization. This approach is beneficial in terms of reducing computational burden and improving the performance in the Bayesian analysis, and this is an acceptable Bayesian-based PBPK optimization method (Hack et al., 2006). The variations of physiological parameters for each species can also be incorporated into the model to generate population simulation results that may be more reflective of the population variability (Li et al., 2017a). Third, the enterohepatic circulation of PFOS is not described in the present model due to limited information about the relevant parameters. In our model structure, the biliary flow from the liver was assumed to enter directly into the feces rather than return into the small intestine for potential enterohepatic circulationin in order to simplify the model and minimize the uncertainty based on earlier PBPK models for PFOA and PFOS (Loccisano et al., 2012; Worley and Fisher, 2015; Worley et al., 2017a, 2017b). However, recent studies have shown that PFOS can bind to liver transporter proteins which may play an important role in enterohepatic circulation (Zhao et al., 2015; Zhao et al., 2017). Also, there are structurally more complex PBPK models for PFOS available in the literature (Loccisano et al., 2011; Fabrega et al., 2014; Fabrega et al., 2016). Once the potential enterohepatic circulation of PFOS has been fully characterized and once additional relevant data are available, the present model can be further improved. Finally, the present model is only for adult animals and humans. Additional studies are needed to extend the model to other life stages, particularly in gestational and lactational periods.

5. Conclusions

In conclusion, the present study developed a comprehensive PBPK model for PFOS in multiple species, including mice, rats, monkeys, and humans. By integrating Bayesian analysis and MCMC algorithm, the uncertainty of model parameters across species was well characterized. The results indicate the efflux transporters in the kidney PTCs may play an important role in the elimination kinetic differences of PFOS between species, which requires experimentation to verify. The present PBPK model can be used to estimate HED and RfD values to support the risk assessment of PFOS. The present model-derived conservative RfD is similar to the guidance value reported by EFSA, but are ~3–6 fold lower than the values recommended by U.S. EPA. Overall, the present model may improve the risk assessment of PFOS, and the open-source code provides a foundation for developing PBPK models for other perfluoroalkyl substances. Additional studies are needed to further improve this model and extend it to other life stages.

Conflict of interest

No conflicts of interest were reported.

Acknowledgments

This study was supported by Kansas State University College of

Veterinary Medicine New Faculty Startup funds. The authors would like to acknowledge Dr. Miao Li from the Institute of Computational Comparative Medicine, Department of Anatomy and Physiology, College of Veterinary Medicine, Kansas State University for assistance in PBPK modeling.

Appendix A. Supplementary data

Supplementary Materials include: (1) detailed explanation on the model equations and codes; (2) additional methods on model calibration, estimation of posterior parameters, and model evaluation; (3) supplementary results including supplementary Tables S1–S3 and Figs. S1–S12; (4) all PBPK model codes in mice, rats, monkeys, and humans, including codes used to generate results presented in Figs. 3–6, Figs. S1–S12, and Tables 3–4; (5) all raw experimental data used in the model calibration and optimization; (6) all raw model-derived simulation data used in the creations of all tables and figures presented in this manuscript, and (7) instructions on how to use the present model. Supplementary Materials to this article can be found online at the journal's website. Supplementary data to this article can be found online at https://doi.org/10.1016/j.envint.2019.03.058.

References

Addis, T., Poo, L.J., Lew, W., 1936. The quantities of protein lost by the various organs and tissues of the body during a fast. J. Biol. Chem. 115, 111–116. http://www.jbc.org/content/115/1/111.full.pdf.

Andersen, M.E., Sarangapani, R., Frederick, C.B., Kimbell, J.S., 1999. Dosimetric adjustment factors for methyl methacrylate derived from a steady-state analysis of a physiologically based clearance-extraction model. Inhal. Toxicol. 11, 899–926. https://doi.org/10.1080/089583799196709.

Andersen, M.E., Green, T., Frederick, C.B., Bogdanffy, M.S., 2002. Physiologically based pharmacokinetic (PBPK) models for nasal tissue dosimetry of organic esters: assessing the state-of-knowledge and risk assessment applications with methyl methacrylate and vinyl acetate. Regul. Toxicol. Pharmacol. 36, 234–245. https://doi.org/10.1006/rtph.2002.1576.

Andersen, M.E., Clewell, H.J., Tan, Y.M., Butenhoff, J.L., Olsen, G.W., 2006. Pharmacokinetic modeling of saturable, renal resorption of perfluoroalkylacids in monkeys - probing the determinants of long plasma half-lives. Toxicology 227, 156–164. https://doi.org/10.1016/j.tox.2006.08.004.

ATSDR, 2018. Toxicological Profile for Perfluoroalkyls. Agency for Toxic Substances and Disease Registry, Atlanta, GA Available. https://www.atsdr.cdc.gov/toxprofiles/tp200.pdf, Accessed date: 28 December 2018.

Beesoon, S., Martin, J.W., 2015. Isomer-specific binding affinity of perfluorooctanesulfonate (PFOS) and perfluorooctanoate (PFOA) to serum proteins. Environ. Sci. Technol. 49, 5722–5731. https://doi.org/10.1021/es505399w.

Bogdanska, J., Borg, D., Sundstrom, M., Bergstrom, U., Halldin, K., Abedi-Valugerdi, M., Bergman, A., Nelson, B., DePierre, J., Nobel, S., 2011. Tissue distribution of S-35-labelled perfluorooctane sulfonate in adult mice after oral exposure to a low environmentally relevant dose or a high experimental dose. Toxicology 284, 54–62. https://doi.org/10.1016/j.tox.2011.03.014.

Bois, F.Y., 2000. Statistical analysis of Fisher et al. PBPK model of trichloroethylene kinetics. Environ. Health Persp. 108, 275–282. https://doi.org/10.1289/ehp.00108s2275.

Bois, F.Y., Gelman, A., Jiang, J., Maszle, D.R., Zeise, L., Alexeef, G., 1996. Population toxicokinetics of tetrachloroethylene. Arch. Toxicol. 70, 347–355. https://doi.org/10.1007/s002040050284.

Brooks, S.P., Roberts, G.O., 1998. Convergence assessment techniques for Markov chain Monte Carlo. Stat. Comput. 8, 319–335. https://doi.org/10.1023/A:1008820505350.

Brown, R.P., Delp, M.D., Lindstedt, S.L., Rhomberg, L.R., Beliles, R.P., 1997. Physiological parameter values for physiologically based pharmacokinetic models. Toxicol. Ind. Health 13, 407–484. https://doi.org/10.1177/074823379701300401.

Butenhoff, J.L., Ehresman, D.J., Chang, S.C., Parker, G.A., Stump, D.G., 2009. Gestational and lactational exposure to potassium perfluorooctanesulfonate (K + PFOS) in rats: developmental neurotoxicity. Reprod. Toxicol. 27, 319–330. https://doi.org/10.1016/j.reprotox.2008.12.010.

Butenhoff, J.L., Chang, S.C., Olsen, G.W., Thomford, P.J., 2012. Chronic dietary toxicity and carcinogenicity study with potassium perfluorooctanesulfonate in Sprague Dawley rats. Toxicology 293, 1–15. https://doi.org/10.1016/j.tox.2012.01.003.

Calafat, A.M., Kuklenyik, Z., Caudill, S.P., Reidy, J.A., Needham, L.L., 2006. Perfluorochemicals in pooled serum samples from United States residents in 2001 and 2002. Environ. Sci. Technol. 40, 2128–2134. https://doi.org/10.1021/es0517973.

Calafat, A.M., Wong, L.Y., Kuklenyik, Z., Reidy, J.A., Needham, L.L., 2007. Polyfluoroalkyl chemicals in the US population: data from the National Health and Nutrition Examination Survey (NHANES) 2003–2004 and comparisons with NHANES 1999–2000. Environ. Health Persp. 115, 1596–1602. https://doi.org/10.1289/ehp.10598.

Chang, S.C., Noker, P.E., Gorman, G.S., Gibson, S.J., Hart, J.A., Ehresman, D.J., Butenhoff, J.L., 2012. Comparative pharmacokinetics of perfluorooctanesulfonate (PFOS) in rats, mice, and monkeys. Reprod. Toxicol. 33, 428–440. https://doi.org/10.1016/j.reprotox.2011.07.002.

Cheng, Y.H., Riviere, J.E., Monteiro-Riviere, N.A., Lin, Z.M., 2018. Probabilistic risk assessment of gold nanoparticles after intravenous administration by integrating in vitro and in vivo toxicity with physiologically based pharmacokinetic modeling. Nanotoxicology 12, 453–469. https://doi.org/10.1080/17435390.2018.1459922.

Chiu, W.A., Ginsberg, G.L., 2011. Development and evaluation of a harmonized physiologically based pharmacokinetic (PBPK) model for perchloroethylene toxicokinetics in mice, rats, and humans. Toxicol. Appl. Pharm. 253, 203–234. https://doi.org/10.1016/j.taap.2011.03.020.

Chiu, W.A., Okino, M.S., Evans, M.V., 2009. Characterizing uncertainty and population variability in the toxicokinetics of trichloroethylene and metabolites in mice, rats, and humans using an updated database, physiologically based pharmacokinetic (PBPK) model, and Bayesian approach. Toxicol. Appl. Pharm. 241, 36–60. https://doi.org/10.1016/j.taap.2009.07.032.

Chiu, W.A., Campbell, J.L., Clewell, H.J., Zhou, Y.H., Wright, F.A., Guyton, K.Z., Rusyn, I., 2014. Physiologically based pharmacokinetic (PBPK) modeling of interstrain variability in trichloroethylene metabolism in the mouse. Environ. Health Persp. 122, 456–463. https://doi.org/10.1289/ehp.1307623.

Choi, K., Chang, J., Lee, M.J., Wang, S., In, K., Galano-Tan, W.C., Jun, S., Cho, K., Hwang, Y.H., Kim, S.J., Park, W., 2016. Reference values of hematology, biochemistry, and blood type in cynomolgus monkeys from Cambodia origin. Lab. Anim. Res. 32, 46–55. https://doi.org/10.5625/lar.2016.32.1.46.

Corley, R.A., Bartels, M.J., Carney, E.W., Weitz, K.K., Soelberg, J.J., Gies, R.A., Thrall, K.D., 2005. Development of a physiologically based pharmacokinetic model for ethylene glycol and its metabolite, glycolic acid, in rats and humans. Toxicol. Sci. 85, 476–490. https://doi.org/10.1093/toxsci/kfi119.

Covington, T.R., Gentry, P.R., Van Landingham, C.B., Andersen, M.E., Kester, J.E., Clewell, H.J., 2007. The use of Markov chain Monte Carlo uncertainty analysis to support a public health goal for perchloroethylene. Regul. Toxicol. Pharmacol. 47, 1–18. https://doi.org/10.1016/j.yrtph.2006.06.008.

Cui, L., Zhou, Q.F., Liao, C.Y., Fu, J.J., Jiang, G.B., 2009. Studies on the toxicological effects of PFOA and PFOS on rats using histological observation and chemical analysis. Arch. Environ. Con. Tox. 56, 338–349. https://doi.org/10.1007/s00244-008-9194-6.

Davies, B., Morris, T., 1993. Physiological-parameters in laboratory-animals and humans. Pharm. Res. 10, 1093–1095. https://doi.org/10.1023/A:1018943613122.

Dong, Z.M., Bahar, M.M., Jit, J., Kennedy, B., Priestly, B., Ng, J., Lamb, D., Liu, Y.J., Duan, L.C., Naidu, R., 2017. Issues raised by the reference doses for perfluorooctane sulfonate and perfluorooctanoic acid. Environ. Int. 105, 86–94. https://doi.org/10.1016/j.envint.2017.05.006.

EFSA, 2015. Scientific opinion on the risks to public health related to the presence of bisphenol A (BPA) in foodstuffs: executive summary. EFSA J. 13, 3978. https://doi.org/10.2903/j.efsa.2015.3978.

EFSA, 2018. Risk to human health related to the presence of perfluorooctane sulfonic acid and perfluorooctanoic acid in food. EFSA J. 16, 5194. https://doi.org/10.2903/j.efsa.2018.5194.

Elcombe, C.R., Elcombe, B.M., Foster, J.R., Chang, S.C., Ehresman, D.J., Butenhoff, J.L., 2012a. Hepatocellular hypertrophy and cell proliferation in Sprague-Dawley rats from dietary exposure to potassium perfluorooctanesulfonate results from increased expression of xenosensor nuclear receptors PPAR alpha and CAR/PXR. Toxicology 293, 16–29. https://doi.org/10.1016/j.tox.2011.12.014.

Elcombe, C.R., Elcombe, B.M., Foster, J.R., Chang, S.C., Ehresman, D.J., Noker, P.E., Butenhoff, J.L., 2012b. Evaluation of hepatic and thyroid responses in male Sprague Dawley rats for up to eighty-four days following seven days of dietary exposure to potassium perfluorooctanesulfonate. Toxicology 293, 30–40. https://doi.org/10.1016/j.tox.2011.12.015.

El-Sheikh, A.A.K., Masereeuw, R., Russel, F.G.M., 2008. Mechanisms of renal anionic drug transport. Eur. J. Pharmacol. 585, 245–255. https://doi.org/10.1016/j.ejphar.2008.02.085.

EPA, 2016a. Drinking Water Health Advisory for Perfluorooctanoic Acid (PFOA) EPA 822-R-16-005. Environmental Protection Agency, Washington, D.C Available. https://www.epa.gov/sites/production/files/2016-05/documents/pfoa_health_advisory_final-plain.pdf, Accessed date: 9 January 2019.

EPA, 2016b. Health Effects Support Document for Perfluorooctane Sulfonate (PFOS). EPA 822-R-16-002. Environmental Protection Agency, Washington, D.C. Available. https://www.epa.gov/sites/production/files/2016-05/documents/pfos_health_advisory_final-plain.pdf, Accessed date: 9 January 2019.

Fabrega, F., Kumar, V., Schuhmacher, M., Domingo, J.L., Nadal, M., 2014. PBPK modeling for PFOS and PFOA: validation with human experimental data. Toxicol. Lett. 230, 244–251. https://doi.org/10.1016/j.toxlet.2014.01.007.

Fabrega, F., Kumar, V., Benfenati, E., Schuhmacher, M., Domingo, J.L., Nadal, M., 2015. Physiologically based pharmacokinetic modeling of perfluoroalkyl substances in the human body. Toxicol. Environ. Chem. 97, 814–827. https://doi.org/10.1080/02772248.2015.1060976.

Fabrega, F., Nadal, M., Schuhmacher, M., Domingo, J.L., Kumar, V., 2016. Influence of the uncertainty in the validation of PBPK models: a case-study for PFOS and PFOA. Regul. Toxicol. Pharmacol. 77, 230–239. https://doi.org/10.1016/j.yrtph.2016.03.009.

Fisher, J.W., Twaddle, N.C., Vanlandingham, M., Doerge, D.R., 2011. Pharmacokinetic modeling: prediction and evaluation of route dependent dosimetry of bisphenol a in monkeys with extrapolation to humans. Toxicol. Appl. Pharm. 257, 122–136. https://doi.org/10.1016/j.taap.2011.08.026.

Food Standards Australia New Zealand (FSANZ), 2016. A critical review of

pharmacokinetic modelling of PFOS and PFOA to assist in establishing HGBVs for these chemicals. Available. http://www.health.gov.au/internet/main/publishing.nsf/content/2200FE086D480353CA2580C900817CDC/$File/7.Critical-Review-Pharmacokinetic-Modelling.pdf, Accessed date: 24 February 2019.

Gelman, A., Bois, F., Jiang, J.M., 1996. Physiological pharmacokinetic analysis using population modeling and informative prior distributions. J. Am. Stat. Assoc. 91, 1400–1412. https://doi.org/10.2307/2291566.

Gelman, D., Koch, C.P., Kosloff, R., 2004. Dissipative quantum dynamics with the surrogate Hamiltonian approach. A comparison between spin and harmonic baths. J. Chem. Phys. 121, 661–671. https://doi.org/10.1063/1.1759312.

Haario, H., Laine, M., Mira, A., Saksman, E., 2006. DRAM: efficient adaptive MCMC. Stat. Comput. 16, 339–354. https://doi.org/10.1007/s11222-006-9438-0.

Hack, C.E., Chiu, W.A., Zhao, Q.J., Clewell, H.J., 2006. Bayesian population analysis of a harmonized physiologically based pharmacokinetic model of trichloroethylene and its metabolites. Regul. Toxicol. Pharmacol. 46, 63–83. https://doi.org/10.1016/j.yrtph.2006.05.012.

Harada, K.H., Hashida, S., Kaneko, T., Takenaka, K., Minata, M., Inoue, K., Saito, N., Koizumi, A., 2007. Biliary excretion and cerebrospinal fluid partition of perfluorooctanoate and perfluorooctane sulfonate in humans. Environ. Toxicol. Phar. 24, 134–139. https://doi.org/10.1016/j.etap.2007.04.003.

Haug, L.S., Thomsen, C., Bechert, G., 2009. Time trends and the influence of age and gender on serum concentrations of perfluorinated compounds in archived human samples. Environ. Sci. Technol. 43, 2131–2136. https://doi.org/10.1021/es802827u.

Hejtmancik, M.R., Ryan, M.J., Toft, J.D., Persing, R.L., Kurtz, P.J., Chhabra, R.S., 2002. Hematological effects in F344 rats and B6C3F1 mice during the 13-week gavage toxicity study of methylene blue trihydrate. Toxicol. Sci. 65, 126–134. https://doi.org/10.1093/toxsci/65.1.126.

Hilgendorf, C., Ahlin, G., Seithel, A., Artursson, P., Ungell, A.L., Karlsson, J., 2007. Expression of thirty-six drug transporter genes in human intestine, liver, kidney, and organotypic cell lines. Drug Metab. Dispos. 35, 1333–1340. https://doi.org/10.1124/dmd.107.014902.

Hsu, V., Vieira, M.D.T., Zhao, P., Zhang, L., Zheng, J.H., Nordmark, A., Berglund, E.G., Giacomini, K.M., Huang, S.M., 2014. Towards quantitation of the effects of renal impairment and probenecid inhibition on kidney uptake and efflux transporters, using physiologically based pharmacokinetic modelling and simulations. Clin. Pharmacokinet. 53, 283–293. https://doi.org/10.1007/s40262-013-0117-y.

ICRP, 2002. Basic anatomical and physiological data for use in radiological protection: reference values. A report of age- and gender-related differences in the anatomical and physiological characteristics of reference individuals. ICRP Publication 89 (32), 5–265 Ann. ICRP.

Iwama, R., Sato, T., Sakurai, K., Takasuna, K., Ichijo, T., Furuhama, K., Satoh, H., 2014. Estimation of glomerular filtration rate in cynomolgus monkeys (Macaca fascicularis). J. Vet. Med. Sci. 76, 1423–1426. https://doi.org/10.1292/jvms.14-0218.

Johnson, J.D., Gibson, S.J., Ober, R.E., 1979. Extent and Route of Excretion and Tissue Distribution of Total Carbon-14 in Rats after a Single Intravenous Dose of Fc-95-14c. Riker Laboratories, Inc, St. Paul, MN (USEPA Docket No. 8(e)HQ-1180-00374).

Kerstner-Wood, C., Coward, L., Gorman, G., 2003. Protein Binding of Perfluorobutane Sulfonate, Perfluorohexane Sulfonate, Perfluorooctane Sulfonate and Perfluorooctanoate to Plasma (Human, Rat and Monkey), and Various Human-Derived Plasma Protein Fractions. U.S. EPA docket AR-226–1354. U.S. Environmental Protection Agency, Washington, DC.

Kim, S.J., Heo, S.H., Lee, D.S., Hwang, I.G., Lee, Y.B., Cho, H.Y., 2016. Gender differences in pharmacokinetics and tissue distribution of 3 perfluoroalkyl and polyfluoroalkyl substances in rats. Food Chem. Toxicol. 97, 243–255. https://doi.org/10.1016/j.fct.2016.09.017.

Kudo, N., Katakura, M., Sato, Y., Kawashima, Y., 2002. Sex hormone-regulated renal transport of perfluorooctanoic acid. Chem. Biol. Interact. 139, 301–316. https://doi.org/10.1016/S0009-2797(02)00006-6.

Lau, C., Thibodeaux, J.R., Hanson, R.G., Rogers, J.M., Grey, B.E., Stanton, M.E., Butenhoff, J.L., Stevenson, L.A., 2003. Exposure to perfluorooctane sulfonate during pregnancy in rat and mouse. II: postnatal evaluation. Toxicol. Sci. 74, 382–392. https://doi.org/10.1093/toxsci/kfg122.

Li, M., Gehring, R., Riviere, J.E., Lin, Z.M., 2017a. Development and application of a population physiologically based pharmacokinetic model for penicillin G in swine and cattle for food safety assessment. Food Chem. Toxicol. 107, 74–87. https://doi.org/10.1016/j.fct.2017.06.023.

Li, Y.J., Cheng, Y.T., Xie, Z.Y., Zeng, F., 2017b. Perfluorinated alkyl substances in serum of the southern Chinese general population and potential impact on thyroid hormones. Sci. Rep. 7. https://doi.org/10.1038/srep43380.

Lin, Z.M., Fisher, J.W., Ross, M.K., Filipov, N.M., 2011. A physiologically based pharmacokinetic model for atrazine and its main metabolites in the adult male C57BL/6 mouse. Toxicol. Appl. Pharm. 251, 16–31. https://doi.org/10.1016/j.taap.2010.11.009.

Lin, Z.M., Fisher, J.W., Wang, R., Ross, M.K., Filipov, N.M., 2013. Estimation of placental and lactational transfer and tissue distribution of atrazine and its main metabolites in rodent dams, fetuses, and neonates with physiologically based pharmacokinetic modeling. Toxicol. Appl. Pharm. 273, 140–158. https://doi.org/10.1016/jtaap.2013.08.010.

Lin, Z.M., Monteiro-Riviere, N.A., Kannan, R., Riviere, J.E., 2016. A computational framework for interspecies pharmacokinetics, exposure and toxicity assessment of gold nanoparticles. Nanomedicine-Uk 11, 107–119. https://doi.org/10.2217/nnm.15.177.

Loccisano, A.E., Campbell, J.L., Andersen, M.E., Clewell, H.J., 2011. Evaluation and prediction of pharmacokinetics of PFOA and PFOS in the monkey and human using a PBPK model. Regul. Toxicol. Pharmacol. 59, 157–175. https://doi.org/10.1016/j.yrtph.2010.12.004.

Loccisano, A.E., Campbell, J.L., Butenhoff, J.L., Andersen, M.E., Clewell, H.J., 2012. Comparison and evaluation of pharmacokinetics of PFOA and PFOS in the adult rat using a physiologically based pharmacokinetic model. Reprod. Toxicol. 33, 452–467. https://doi.org/10.1016/j.reprotox.2011.04.006.

Luebker, D.J., Case, M.T., York, R.G., Moore, J.A., Hansen, K.J., Butenhoff, J.L., 2005. Two-generation reproduction and cross-foster studies of perfluorooctanesulfonate (PFOS) in rats. Toxicology 215, 126–148. https://doi.org/10.1016/j.tox.2005.07.018.

Martin, M.T., Brennan, R.J., Hu, W.Y., Ayanoglu, E., Lau, C., Ren, H.Z., Wood, C.R., Corton, J.C., Kavlock, R.J., Dix, D.J., 2007. Toxicogenomic study of triazole fungicides and perfluoroalkyl acids in rat livers predicts toxicity and categorizes chemicals based on mechanisms of toxicity. Toxicol. Sci. 97, 595–613. https://doi.org/10.1093/toxsci/kfm065.

Mirfazaelian, A., Kim, K.B., Anand, S.S., Kim, H.J., Tornero-Velez, R., Bruckner, J.V., Fisher, J.W., 2006. Development of a physiologically based pharmacokinetic model for deltamethrin in the adult male Sprague-Dawley rat. Toxicol. Sci. 93, 432–442. https://doi.org/10.1093/toxsci/kfl056.

Olsen, G.W., Church, T.R., Miller, J.P., Burris, J.M., Hansen, K.J., Lundberg, J.K., Armitage, J.B., Herron, R.M., Medhdizadehkashi, Z., Nobiletti, J.B., O'Neill, E.M., Mandel, J.H., Zobel, L.R., 2003a. Perfluorooctanesulfonate and other fluorochemicals in the serum of American red Cross adult blood donors. Environ. Health Persp. 111, 1892–1901. https://doi.org/10.1289/ehp.6316.

Olsen, G.W., Hansen, K.J., Stevenson, L.A., Burris, J.M., Mandel, J.H., 2003b. Human donor liver and serum concentrations of perfluorooctanesulfonate and other perfluorochemicals. Environ. Sci. Technol. 37, 888–891. https://doi.org/10.1021/es020955c.

Olsen, G.W., Burris, J.M., Ehresman, D.J., Froehlich, J.W., Seacat, A.M., Butenhoff, J.L., Zobel, L.R., 2007. Half-life of serum elimination of perfluorooctanesulfonate, perfluorohexanesulfonate, and perfluorooctanoate in retired fluorochemical production workers. Environ. Health Persp. 115, 1298–1305. https://doi.org/10.1289/ehp.10009.

Olsen, G.W., Mair, D.C., Church, T.R., Ellefson, M.E., Reagen, W.K., Boyd, T.M., Herron, R.M., Medhdizadehkashi, Z., Nobilett, J.B., Rios, J.A., Butenhoff, J.L., Zobel, L.R., 2008. Decline in perfluorooctanesulfonate and other polyfluoroalkyl chemicals in American red Cross adult blood donors, 2000-2006. Environ. Sci. Technol. 42, 4989–4995. https://doi.org/10.1021/es800071x.

Qi, Z.H., I, W., Mehta, A., Jin, J.P., Zhao, M., Harris, R.C., Fogo, A.B., Breyer, M.D., 2004. Serial determination of glomerular filtration rate in conscious mice using FITC-inulin clearance. Am. J. Physiol. Renal Physiol. 286, F590–F596. https://doi.org/10.1152/ajprenal.00324.2003.

Seacat, A.M., Thomford, P.J., Hansen, K.J., Olsen, G.W., Case, M.T., Butenhoff, J.L., 2002. Subchronic toxicity studies on perfluorooctanesulfonate potassium salt in cynomolgus monkeys. Toxicol. Sci. 68, 249–264. https://doi.org/10.1093/toxsci/68.1.249.

Seacat, A.M., Thomford, P.J., Hansen, K.J., Clemen, L.A., Eldridge, S.R., Elcombe, C.R., Butenhoff, J.L., 2003. Sub-chronic dietary toxicity of potassium perfluorooctanesulfonate in rats. Toxicology 183, 117–131. https://doi.org/10.1016/S0300-483x(02)00511-5.

Soetaert, K., Petzoldt, T., 2010. Inverse modelling, sensitivity and Monte Carlo analysis in R using package FME. J. Stat. Softw. 33, 1–28. https://doi.org/10.18637/jss.v033.i03.

Tan, Y.M., Clewell, H.J., Andersen, M.E., 2008. Time dependencies in perfluorooctylacids disposition in rat and monkeys: a kinetic analysis. Toxicol. Lett. 177, 38–47. https://doi.org/10.1016/j.toxlet.2007.12.007.

Thibodeaux, J.R., Hanson, R.G., Rogers, J.M., Grey, B.E., Barbee, B.D., Richards, J.H., Butenhoff, J.L., Stevenson, L.A., Lau, C., 2003. Exposure to perfluorooctane sulfonate during pregnancy in rat and mouse. I: maternal and prenatal evaluations. Toxicol. Sci. 74, 369–381. https://doi.org/10.1093/toxsci/kfg121.

Wambaugh, J.F., 2018. Comment on: Dong et al. (2017) "Issues raised by the reference doses for perfluorooctonate sulfonate and perfluorooctanoic acid". Environ. Int. 121, 1372–1374. https://doi.org/10.1016/j.envint.2018.10.048.

Wambaugh, J.F., Setzer, R.W., Pitruzzello, A.M., Liu, J., Reif, D.M., Kleinstreuer, N.C., Wang, N.C.Y., Sipes, N., Martin, M., Das, K., DeWitt, J.C., Strynar, M., Judson, R., Houck, K.A., Lau, C., 2013. Dosimetric anchoring of in vivo and in vitro studies for perfluorooctanoate and perfluorooctanesulfonate. Toxicol. Sci. 136, 308–327. https://doi.org/10.1093/toxsci/kft204.

Wan, H.T., Zhao, Y.G., Wei, X., Hui, K.Y., Giesy, J.P., Wong, C.K.C., 2012. PFOS-induced hepatic steatosis, the mechanistic actions on beta-oxidation and lipid transport. Bba-Gen Subjects 1820, 1092–1101. https://doi.org/10.1016/j.bbagen.2012.03.010.

Wang, L., Wang, Y., Liang, Y., Li, J., Liu, Y.C., Zhang, J., Zhang, A.Q., Fu, J.J., Jiang, G.B., 2014. PFOS induced lipid metabolism disturbances in BALB/c mice through inhibition of low density lipoproteins excretion. Sci. Rep. 4. https://doi.org/10.1038/srep04582.

Weaver, Y.M., Ehresman, D.J., Butenhoff, J.L., Hagenbuch, B., 2010. Roles of rat renal organic anion transporters in transporting perfluorinated carboxylates with different chain lengths. Toxicol. Sci. 113, 305–314. https://doi.org/10.1093/toxsci/kfp275.

World Health Organization, International Programme on Chemical Safety, Geneva, Switzerland, 2010. Characterization and Application of Physiologically Based Pharmacokinetic Models in Risk Assessment. Available. https://www.who.int/ipcs/methods/harmonization/areas/pbpk_models.pdf, Accessed date: 8 January 2019.

Worley, R.R., Fisher, J., 2015. Application of physiologically-based pharmacokinetic modeling to explore the role of kidney transporters in renal reabsorption of perfluorooctanoic acid in the rat. Toxicol. Appl. Pharm. 289, 428–441. https://doi.org/10.1016/j.taap.2015.10.017.

Worley, R.R., Moore, S.M., Tierney, B.C., Ye, X.Y., Calafat, A.M., Campbell, S., Woudneh, M.B., Fisher, J., 2017a. Per- and polyfluoroalkyl substances in human serum and

urine samples from a residentially exposed community. Environ. Int. 106, 135–143. https://doi.org/10.1016/j.envint.2017.06.007.

Worley, R.R., Yang, X.X., Fisher, J., 2017b. Physiologically based pharmacokinetic modeling of human exposure to perfluorooctanoic acid suggests historical non drinking-water exposures are important for predicting current serum concentrations. Toxicol. Appl. Pharm. 330, 9–21. https://doi.org/10.1016/j.taap.2017.07.001.

Yang, C.H., Glover, K.P., Han, X., 2010a. Characterization of cellular uptake of perfluorooctanoate via organic anion-transporting polypeptide 1A2, organic anion transporter 4, and urate transporter 1 for their potential roles in mediating human renal reabsorption of perfluorocarboxylates. Toxicol. Sci. 117, 294–302. https://doi.org/10.1093/toxsci/kfq219.

Yang, Y., Xu, X., Georgopoulos, P.G., 2010b. A Bayesian population PBPK model for multiroute chloroform exposure. J. Expo. Sci. Environ. Epidemiol. 20, 326–341. https://doi.org/10.1038/jes.2009.29.

Yang, X.X., Doerge, D.R., Teeguarden, J.G., Fisher, J.W., 2015. Development of a physiologically based pharmacokinetic model for assessment of human exposure to bisphenol A. Toxicol. Appl. Pharm. 289, 442–456. https://doi.org/10.1016/j.taap.2015.10.016.

Yoon, M., Nong, A., Clewell, H.J., Taylor, M.D., Dorman, D.C., Andersen, M.E., 2009. Evaluating placental transfer and tissue concentrations of manganese in the pregnant rat and fetuses after inhalation exposures with a PBPK model. Toxicol. Sci. 112, 44–58. https://doi.org/10.1093/toxsci/kfp198.

Zhao, W., Zitzow, J.D., Ehresman, D.J., Chang, S.C., Butenhoff, J.L., Forster, J., Hagenbuch, B., 2015. Na+/taurocholate cotransporting polypeptide and apical sodium-dependent bile acid transporter are involved in the disposition of perfluoroalkyl sulfonates in humans and rats. Toxicol. Sci. 146, 363–373. https://doi.org/10.1093/toxsci/kfv102.

Zhao, W., Zitzow, J.D., Weaver, Y., Ehresman, D.J., Chang, S.C., Butenhoff, J.L., Hagenbuch, B., 2017. Organic anion transporting polypeptides contribute to the disposition of perfluoroalkyl acids in humans and rats. Toxicol. Sci. 156, 84–95. https://doi.org/10.1093/toxsci/kfw236.